Emergent Materials (2022) 5:1133–1155
https://doi.org/10.1007/s42247-021-00312-4

ORIGINAL ARTICLE

Investigation on Co(II), Ni(II), Cu(II) and Zn(II) complexes derived from novel *N*′-(3-hydroxybenzoyl)thiophene-2-carbohydrazide: structural characterization, electrochemical detection of biomolecules, molecular docking and biological evaluation

Lubna Afroz[1] · M. H. Moinuddin Khan[1] · H. M. Vagdevi[2] · Malathesh Pari[2] · R. Mohammed Shafeeualla[3] · K. M. Mussuvir Pasha[4]

Received: 16 July 2021 / Accepted: 25 September 2021 / Published online: 4 November 2021

Abstract
A series of transition metal (Co(II), Ni(II), Cu(II) and Zn(II)) complexes of novel *N*′-(3-hydroxybenzoyl)thiophene-2-carbohydrazide ligand was synthesized and their structures were confirmed using ^{1}H,^{13}C NMR, IR, UV–visible, mass spectra, magnetic susceptibility, thermogravimetric analysis (TGA) and powder XRD techniques. The results obtained by the above mentioned techniques justified the promising bidendate coordination of the synthesized ligand and octahedral geometry was proposed to all the metal-coordinated compounds. In addition, with the help of cyclic voltammogram, the electrocatalysis ability of Co(II) HTC/GCE was examined utilizing different concentrations of dopamine (DA) and uric acid (UA). The Co(II)HTC/GCE sensor showed an excellent electrochemical performance with DA and UA at the concentration ranges 0.2 to 10 μML^{-1} and 0.1 to 0.8 μML^{-1} with detection limits (LOD) of 0.066 μML^{-1} and 0.333 μML^{-1} and sensitivities of 1.069 $\mu A\mu M^{-1}$ cm^{-2} and 5.170 $\mu A\mu M^{-1}$ cm^{-2} for DA and UA. Thus, the modified electrode exhibited better performance, extended shelf life, better reduplication and procreation. Further, bioefficacies of prepared ligand and its metal-coordinated compounds were examined against the bacteria (*Staphylococcus aureus*, *Escherichia coli*, *Salmonella typhi*, and *Bacillus subtilis*) and fungi (*Aspergillus niger* and *Candida albicans*) strains using standard procedures. Moreover, the ligand and its metal complexes were evaluated for the antioxidant and cytotoxic studies on four different strain of cells (MCF-7, HeLa, K-562, and Vero) where Co(II) and Cu(II)coordinated compounds revealed admirable cytotoxity for MCF-7 and Hela cell lines. Lastly, molecular docking studies were performed on cancer receptors for the determination of binding mode of ligand and its transition metal complexes.

Keywords Transition metals · Spectral study · Electrochemistry · Biomolecules · Biological applications · Molecular docking · Cytotoxic

1 Introduction

In the previous two decades, the appearance and variety of hazardous diseases has expanded. This is due to the existence of drug-defiant unfeasible bacterial strains which has become very bothersome in the society. Hence in the present scenario, the necessity to develop advanced, sophisticated, and novel synthetic compounds with antimicrobial properties is considered a significant area of studies all over the globe [1]. Apart from antimicrobial infections, greater efforts have been invested by chemists and pharmacists to identify the molecules bearing anti-cancer properties. This is because cancer is considered the main source of mortality

✉ M. H. Moinuddin Khan
drmk@jnnce.ac.in

[1] Department of Chemistry, JNN College of Engineering (VTU), Shimoga, Karnataka, India

[2] Department of Chemistry, Sahyadri Science College, Kuvempu University, Shimoga, Karnataka, India

[3] Department of Chemistry, Sir.M.V.Science College, Kuvempu University, Shimoga, Karnataka, India

[4] Department of Chemistry, Vijayanagara Sri Krishnadevaraya University, Ballari, Karnataka, India

around the globe and specifically India enlists more than 1.1 million new cases out of 14 million cases every 12 months consistently. It is also predicted that by 2030, the hazard of cancer will be extreme as there will be 26 million new cases causing 17 million deaths [2]. On the other hand, although there is an extensive progress in chemotherapy of cancer, there are certain undesirable side effects associated with available cancer treatments which includes alopecia, bone marrow depression, drug actuated cancers, and also genotoxicity. Hence there is an absolute need to outline and synthesize newer and safer group of anticancer agents to overcome the threat imposed by cancer [3, 4].

Due to their deficient d-shells, transition metals bond to the surrounding cluster of molecules or ions to form metal complexes of coordination compounds [5]. Furthermore, hydrazides [R-CO–NH-NH_2] and their analogues have continued to attract interest due to their ability to coordinate with different transition metals. There are many enduring documented confirmations reporting about the enormous number of hydrazides and their complexes showcasing distinct biological activities [6–10]. In both medicinal chemistry and organic chemistry, heterocyclic compounds play a fundamental role because of their endless biological action. One such heterocycle is thiophene and its compounds which have gained the tag of the "wonder heterocycle" due to its wide scope of biological properties which includes antioxidant, anti-HIV, bactericidal, antifungal, anti-inflammatory and antitumor [11–18].

Cyclic voltammogram is described as potentiodynamic electrochemical study, which is known to be simple, cost-effective, quick and trustable to detect the molecules. This method is utilized to investigate the electrocatalytic nature of an analyte in liquid media or of the compound adsorbed on the electrode surface [19]. Over the years, precise and real-time detection of biomolecules, sludges, and toxic materials has gained considerable significance in the scientific community. Dopamine (DA) being one such molecule is a monoamine compound and also an essential adrenaline-secreting molecule among vertebrate's nervous system and the outcome of low levels of DA in neurocytes leads to critical conditions like schizophrenic psychosis and Parkinsonism disorders. Hence the concentration of DA in body fluids has to be observed frequently with the help of a facile and reliable technique [20]. Another biomolecule, uric acid (UA), is the main resultant substance formed due to the metabolic process of purine. The unusual proportion of this biomolecule results in numerous diseases like hyperuricemia, gout and leukemia [21]. The current study illustrates the use of synthesized Co(II) complex for the electrochemical detection of the aforementioned bioanalytes.

From the above-mentioned findings, it is clear that in spite of greater attention being provided to analyze the metal complexes derived from hydrazides and thiophene moieties, no reports have appeared in the literature describing the single-step synthesis of ligand N^1-(2-hydroxybenzoyl)thiophene-2-carbohydrazide derived from aforesaid organic moieties. Further, to the best of our knowledge, there are no investigations reported describing the characterization, electrochemical studies of biomolecules, and biological evaluation of transition metal complexes of ligand N^1-(2-hydroxybenzoyl) thiophene-2-carbohydrazide. Moreover, due to the pressing need for new therapeutic drugs to treat cancer illness, metal complexes of prior-mentioned ligand have been tested for their effectiveness against four different cancer cell lines. Thus, the following content involves the study of the synthesis of novel ligand N^1-(2-hydroxybenzoyl)thiophene-2-carbohydrazide (HTC) and its transition metal complexes derived from benzohydrazide and thiophenecarbonyl chloride. Further, they are examined with the help of varied spectral procedures, powder X-ray diffraction, CV technique and thermoanalytical methods. This study also aimed to explore the pharmacological potency of both ligand and its metal-coordinated compounds including antibacterial, antifungal, DPPH free radical assay and cytotoxic activity. Binding affinity of ligand and its metal-coordinated compounds with target protein were determined via molecular docking study.

2 Experimental

2.1 Materials and instrumentation

Each of the chemicals and solvents utilized in the current work were refined and AR grade. Benzohydrazide, thiophenecarbonyl chloride, trimethylamine and dichloromethane were obtained from Sigma–Aldrich and from Hi-Media entire metal salts were bought and utilized as received without further purification. On an electrothermal melting factor device, melting points were documented and were noncorrected. With the aid of Bruker at 400 MHz spectrometer, ^{1}H and ^{13}C NMR spectra were determined. Using tetramethylsilane (TMS) as the internal standard, chemical shifts are given in δ values (ppm). Molecular weights of unknown compounds were obtained by LC–MS spectroscopy at Centralized Instrumentation Facility, Mysore University, Karnataka, India. By Perkin-Elmer 2400 Series II analyzer, elemental analysis (C, H, and N) was carried out. In the range of 250–4000 cm^{-1}, infrared spectra were reported using Perkin Elmer spectrophotometer with KBr pellets. At room temperature, magnetic susceptibilities were determined by making use of Gouy method. In the solution of DMF (10^{-3}), the molar conductivity of the metal complex was measured with the Equip-tronics EQ-660A conductivity meter.

Absorbance was found by the Systronics UV–vis spectrometer-119, X-ray diffractometer (Rigaku Miniflex 600, 5th gen) with Cu-K_α radiation (wavelength 0.154 nm),

and from room temperature to 850 °C at a heating pace of 20 °C min^{-1} (20 mL min^{-1}), thermogravimetric analysis (TGA) analysis of metal complexes was determined by SDT Q600 V20.9 Build 20 in a nitrogen atmosphere at SAIF, Karnataka University, Dharwad. Electrochemical experiments (cyclic voltammetry) were carried out with an CH instruments, electrochemical analyzer CHI608D made in the USA at JNNCE College, Shimoga.

2.2 Synthesis of ligand N^1-(2-hydroxybenzoyl) thiophene-2-carbohydrazide (HTC) (5)

An equimolar ratio of benzohydrazide (1) (0.003 mol) and thiophenecarbonyl chloride (2) (0.003 mol) were taken in a round bottomed flask to which catalytic amount of (0.004 mol) trimethylamine was added dropwise to the abovementioned reaction mixture in the presence of dichloromethane as a solvent. In the next step, the aforesaid reaction mixture was stirred for 5 h at room temperature. After the completion of reaction, a colorless solid precipitate was collected by filtration, washed with ethanol, recrystallized from ethanol and was made to dry over $CaCl_2$ in a desiccator. The reaction sequence is depicted in Fig. 1.

Data of ligand (HTC): Colorless solid, yield: 78%, M.P. 155–157 °C, IR (KBr, cm^{-1}): 3429 (υ -OH), 3207 (υ -NH), 2354 (υ Ar CH), 1633 (υ C = O), 744 (υ C-S); ^{1}H NMR (DMSO-d6) ppm: δ11.88 (bs, 1H, OH), δ10.59, 11.27 (bs, 2H, NH), δ7.87–7.91 (m, Ar-3H, thiophene), δ7.48–6.94 (m, Ar-4H, benzene); LC–MS mass found (calculated) for ($C_{12}H_{10}N_2O_3S$) = 263 (M + 1) (262.28).

2.3 General procedure for the synthesis of metal complexes

To the warm ethanolic solution of ligand HTC (0.002 mol), addition of warm ethanolic solution of (0.001 mol) $MCl_2.0.6H_2O$ (Co, Ni, Cu, Zn) metal chloride was done in dropwise manner upon continuous stirring followed by adding up of few drops of triethylamine. Then the reaction mixture was further stirred and on a water bath it was refluxed for about 7–8 h. The procured hot solution was cooled to room temperature. Then the colored precipitates obtained were separated by filtration, washed thoroughly with distilled water as well as cold ethanol and lastly were made to dry over anhydrous $CaCl_2$ in an vacuum desiccator. The preparation of metal complex is represented in Fig. 2.

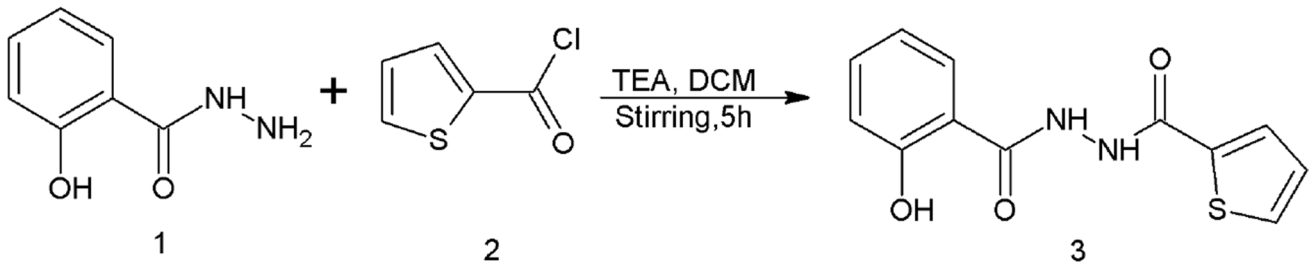

Fig. 1 **1** Benzohydrazide, **2** thiophenecarbonyl chloride, and **3** N^1-(2-hydroxybenzoyl)thiophene-2-carbohydrazide (L)

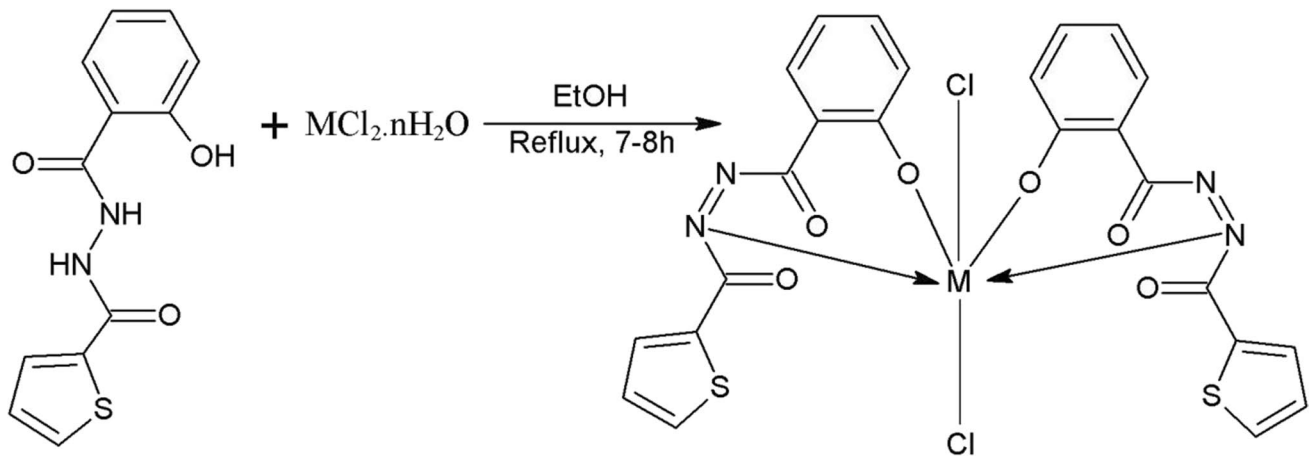

Fig. 2 Synthesis of metal complexes (M = Co, Ni, Cu, and Zn)

2.3.1 [Co(HTC)$_2$.Cl$_2$] complex

Grayish brown solid, yield: 53%, M.P. 272–274 °C, elemental analysis (%) found (calculated) for $C_{24}H_{14}O_6Cl_2N_4S_2Co$: C-44.22(44.46), H-2.11(2.18), N-8.59(8.64), Co-9.00(9.08); IR (KBr) (cm^{-1}): 2368 (υ Ar CH), 1641 (υ C = O), 1541 (υ N = N), 748 (υ C-S), 538 (υ M–O), 432 (υ M–N); LC–MS mass found (calculated) for ($C_{24}H_{14}Cl_2CoN_4O_6S_2$) = 649.02 (M + 1) (648.35); UV–vis: λ_{max} in (nm): 619, 708; conductance (Ω^{-1} cm^2 mol^{-1}): 22.

2.3.2 [Ni(HTC)$_2$.Cl$_2$] complex

Grayish green solid, yield: 59%, M.P. 262–264 °C, elemental analysis (%) found (calculated) for $C_{24}H_{14}O_6Cl_2N_4S_2Ni$: C-44.38(44.48), H-2.08(2.18), N-8.55(8.64), Ni-9.01(9.05); IR (KBr) (cm^{-1}): 2359 (υ Ar CH), 1637 (υ C = O), 1539 (υ N = N), 748 (υ C-S), 540 (υ M–O), 432 (υ M–N); LC–MS mass found (calculated) for ($C_{24}H_{14}Cl_2NiN_4O_6S_2$) = 649.18 (M + 1) (648.11); UV–vis: λ_{max} in (nm): 479, 514, 618; conductance (Ω^{-1} cm^2 mol^{-1}): 19.

2.3.3 [Cu(HTC)$_2$.Cl$_2$] complex

A light green solid, yield: 56%, M.P. 270–273 °C, elemental analysis (%) found (calculated) for $C_{24}H_{14}O_6Cl_2N_4S_2Cu$: C-43.92(44.15), H-2.09(2.16), N-8.49(8.58), Cu-9.65(9.73); IR (KBr) (cm^{-1}): 2336 (υ Ar CH), 1633 (υ C = O), 1542 (υ N = N), 750 (υ C-S), 524 (υ M–O), 430 (υ M–N); LC–MS mass found (calculated) for ($C_{24}H_{14}Cl_2CuN_4O_6S_2$) = 653.86 (M + 1) (652.96); UV–vis: λ_{max} in (nm): 538; conductance (Ω^{-1} cm^2 mol^{-1}): 28.

2.3.4 [Zn(HTC)$_2$.Cl$_2$] complex

Colorless solid, yield: 62%, M.P. 276–278 °C, elemental analysis (%) found (calculated) for $C_{24}H_{14}O_6Cl_2N_4S_2Zn$: C-44.02(44.11), H-2.11(2.16), N-8.49(8.56), Zn-9.54(9.98); IR (KBr) (cm^{-1}): 3016 (υ Ar–CH), 1630 (υ C = O), 1546 (υ N = N), 750 (υ C-S), 540 (υ M–O), 432 (υ M–N); LC–MS mass found (calculated) for ($C_{24}H_{14}Cl_2ZnN_4O_6S_2$) = 655.02 (M + 1) (654.80); conductance (Ω^{-1} cm^2 mol^{-1}): 31.

2.4 Electrochemistry

Electrochemical experiments (cyclic voltammetry) were carried out with electrochemical analyzer CHI608D (USA) using typical tri-electrode system consisting of glassy carbon electrode (GCE) as working electrode, platinum wire as counter, and Ag/AgCl reference electrode. The outer surface area of GCE was cleansed via 0.3 and 0.05mm alumina slurries and ultrasonicated in refined water and DMF, respectively. As a next step by flushing N_2, the bare GCE was subjected to drying and the polished GCE was utilized in order to modify the surface. Finally, the complex mounted on cleansed GCE was utilized as working electrode. The electrocatalysis behavior of Co(II) complex was evaluated with the aid of cyclic voltammogram utilizing modified GCE for varied amounts of DA and UA.

2.5 Antimicrobial activity

2.5.1 Antibacterial screening

The ligand HTC and its metal-coordinated compounds were evaluated for their antibacterial activity against four various bacterial strains like *Staphylococcus aureus*, *Escherichia coli*, *Bacillus subtilis*, and *Salmonella Typhi* via agar well–diffusion procedure. A 24-old Muller-Hinton broth culture of the test bacteria was applied to a cleansed Muller-Hinton agar plate with sterilized cotton, followed by punching a 9-mm well using a sterile cork borer. The drug chloramphenicol was used as a standard at two various amounts (100 and 200 µg/mL in 10% DMSO) and control (10% DMSO) was introduced to specified labeled wells. The plates were left to stand for around 30 min and at 37 °C they were incubated for 24 h in an upstanding position [22]. Further test solution was observed to diffuse during this period and zone of inhibitions were recorded using vernier calipers.

2.5.2 Antifungal screening

The ligand HTC and its metal-coordinated compounds were evaluated for their antifungal activity against *Candida albicans* and *Aspergillus niger* fungi utilizing sabouraud dextrose agar diffusion procedure [22]. With a cleansed cork borer, wells were prepared (9 mm diameter). Standard drug (fluconazole, 100 g/mL clean refined water) and control (10% DMSO) were added to individually labeled wells. One hundred forty microliters from each (100 and 200 µg/mL in 10% DMSO) of the test stock solution of the compounds was introduced to these wells and the plates were permitted to stand for an hour to speed up the dissipation process. At 37 °C, the plates were inoculated for 48 h and toward the end of the inoculation period, the diameter of the zone of inhibition around the wells was estimated with vernier calipers.

2.6 Minimum inhibitory concentration (MIC)

The uncoordinated ligand HTC and its metal complexes were screened for antimicrobial activity using the methods as mentioned in the literature. Using the serial dilution technique, MIC of the most active complexes were examined. The MIC analysis of the synthesized ligand and its metal complexes on two bacterial strains as well as two fungal strains at different concentrations, i.e., 100, 50, 25, and 12.5 mg/mL, were

studied. The observations obtained by the MIC are discussed in Tables 11 and 12.

2.7 Antioxidant activity

The antioxidant activity of the synthesized ligands and their metal chelates was carried out according to the literature utilizing the DPPH technique [23, 24]. The compound was dissolved in various quantities in methanol and filled into 5mL vials. To these test vials, 3 mL of 0.004% DPPH in methanol was added and the mixtures were incubated in the dark at room temperature for 30 min. Ascorbic acid was considered the standard. From an outer source, if DPPH abstracts hydrogen radical, the absorption declines stoichiometrically based on the total quantity of electrons or hydrogen atoms. By using the following equation, DPPH scavenging activity is calculated and absorbance was estimated at 517 nm. The data obtained are discussed in Table 13, respectively.

$$\text{Scavenging ratio } (\%) = \left[(\text{Ai} - \text{Ao})/(\text{Ac} - \text{Ao})\right] \times 100\%$$

where A_i is the absorbance in the presence of the check compound, A_o is absorbance of the blank in the absence of the check compound, and A_c is the absorbance in the absence of the test compound.

2.8 Molecular docking studies

Molecular docking being a beneficial supplementary tool is utilized to comprehend the extent of interaction of synthesized materials with receptor sites. For the prepared compounds, molecular docking was done as per the reported procedure [25]. Throughout the entire research work, Hex molecular modeling package version 8.2 was used and also the three-dimensional crystal structure of epidermal growth factor receptor (EGFR) tyrosine kinase domain PDB code: 2A91 was utilized in the current work. The ligand was changed discretely to energy-minimized 2D or 3D conformations with Hex 3D Ultra 8.2 and those conformations were conceived with the Acceryl Discovery Studio 3.1 client. On the anticancer receptor of PDB code: 2A91, the in-silico molecular docking was performed using actinoin as the reference for docking studies. The crystal structure of the receptor has been obtained via protein data bank and entire water molecules and heteroatoms were removed before screening for docking studies. Further the observed docking values persuaded us for conducting wet analysis of cytotoxic activity which are enlisted in Table 14.

2.9 Cytotoxicity assay [cell preparation and cell viability]

Cell toxicity of the synthesized HTC compound and its metal coordinated compounds were examined against four different strains of cells like MCF-7, Vero, Hela, and K-562 by adopting MTT assay method [25]. The strains of cells were conceived via National Centre for Cell Science, Pune, India and Dulbecco's modified Eagle medium (DMEM) was used for cultivation of cell lines provided with 10% fetal bovine serum, and also 1% penicillin and streptomycin were used for growth of cell. Selected cell lines were cultured in humid incubator at 37 °C in 5% CO_2 atmosphere. The cells were sown in 96-well plate (10,000 cells per well), the plates were inoculated for a day, followed by the addition of 100 µL medium containing various concentrations of tested compounds which were re-inoculated for 24 h. Untreated cells were considered control. Toward the final stage of the treatment, addition of 10 µL of 3–4,5-dimethylthiazole-2,5-diphenyltetraazolium bromide (MTT) to each plate was done and incubated for about 2–3 h in 5% CO2 atmosphere. The developed crystals of formazan were dissolved in 150 µL DMSO and the absorbance was noted at 570 nm. The cytotoxic result was estimated using the following equations:

$$\text{Cytotoxicity } (\%) = 1 - (\text{Mean absorbance of test compound}/\text{Mean absorbance of} - \text{ve control}) \times 100$$

$$\text{Cell viability } \% = 100 - \text{Cytotoxicity } \%$$

3 Results and discussion

3.1 Chemistry

The ligand HTC was synthesized via mixing of benzohydrazide and thiophenecarbonyl chloride in the presence of triethylamine as a catalyst. The physical and chemical properties of both ligand and its metal complexes were observed to be unchanged under atmospheric conditions. The ligand and its metal complexes were observed to be stable under atmospheric conditions, soluble in polar organic solvents, and partially soluble in common organic solvents. The analytical and physical data of ligand and its metal coordinated compounds are represented in Table 1. By the analytical results, it was confirmed that the metal to ligand ratio in all complexes was 1:2. The molar conductivity values of all the metal coordinated compounds were evaluated at room temperature in DMF solution at a concentration of 0.001 M. In the range of 19–31 $\Omega^{-1}cm^2mol^{-1}$ the conductivity data of metal complexes were obtained specifying the non-electrolytic behavior of complexes.

Table 1 Physical properties and analytical data of the ligand and their complexes

Compounds	Mol. wt	% yield	CHN % analysis found (calculated)				Molar conductance (Ω^{-1} cm^2 mol^{-1})	M.P. (°C)
			M	C	N	H		
$C_{12}H_{10}N_2O_3S$ (HTC) colorless	262.28	78	-	54.94 (54.87)	10.68 (10.64)	3.84 (3.79)	-	155–157
$[Co(HTC)_2.Cl_2]$(**1**) grayish brown	648.35	53	9.08	44.46 (44.22)	8.64 (8.59)	2.18 (2.11)	22	272–274
$[Ni(HTC)_2.Cl_2]$(**2**) pale green	648.11	59	9.05	44.48 (44.38)	8.64 (8.55)	2.18 (2.08)	19	262–264
$[Cu(HTC)_2.Cl_2]$(**3**) light green	652.96	56	9.73	44.15 (43.92)	8.58 (8.49)	2.16 (2.09)	28	270–273
$[Zn(HTC)_2.Cl_2]$(**4**) colorless	654.80	62	9.98	44.11 (44.02)	8.56 (8.49)	2.16 (2.11)	31	276–278

3.2 ^{1}H NMR and ^{13}C NMR spectral studies

The ^{1}H NMR spectrum of HTC showed a broad singlet at 11.88 ppm for –OH proton (bs,1H,OH); while two broad singlets at 11.27 ppm and 10.59 ppm were obtained for two –NH protons. The peaks obtained in the range 7.87–7.91 ppm were denoted as the aromatic protons of the thiophene ring (m, Ar-3H, thiophene) and the peaks observed in the region 7.48–6.94 ppm were prescribed as the aromatic protons of the benzene ring (m, Ar-4H, benzene), respectively.

The ^{13}C NMR spectrum of the synthesized ligand indicated twelve carbon atoms in different environment ranging from 168.30 to 115.06 ppm, respectively. The two peaks resonated at 168.30 and 161.06 ppm were assigned to carbonyl carbon of the ligand molecule which is considered to be the most de-shielded carbon in the molecule. The peak observed at 159.66 ppm was referred to the carbon linked to the hydroxyl group of the benzene ring. The rest of the carbon atoms of thiophene were attributed to the peaks at 137.45, 134.70, 132.31 and 129.70 ppm and the carbon atoms of benzene ring were assigned to the peaks obtained at 128.80, 128.69, 119.58, 117.87 and 115.06 ppm. Thus, it is clear from the overall observations that the spectral data of both ^{1}H NMR and ^{13}C NMR closely match the molecular structure of the proposed ligand. The spectra of both ^{1}H NMR and ^{13}C NMR are shown in Figs. 3 and 4.

3.3 Mass spectral studies

The mass spectra of ligand justify the expected formula and displayed well-specified molecular ion peak [M + 1] at *m*/*z* 263.00 (cal: 262.28) as depicted in Fig. 5. Also the mass spectra of all the metal complexes $[Co(HTC)_2$.

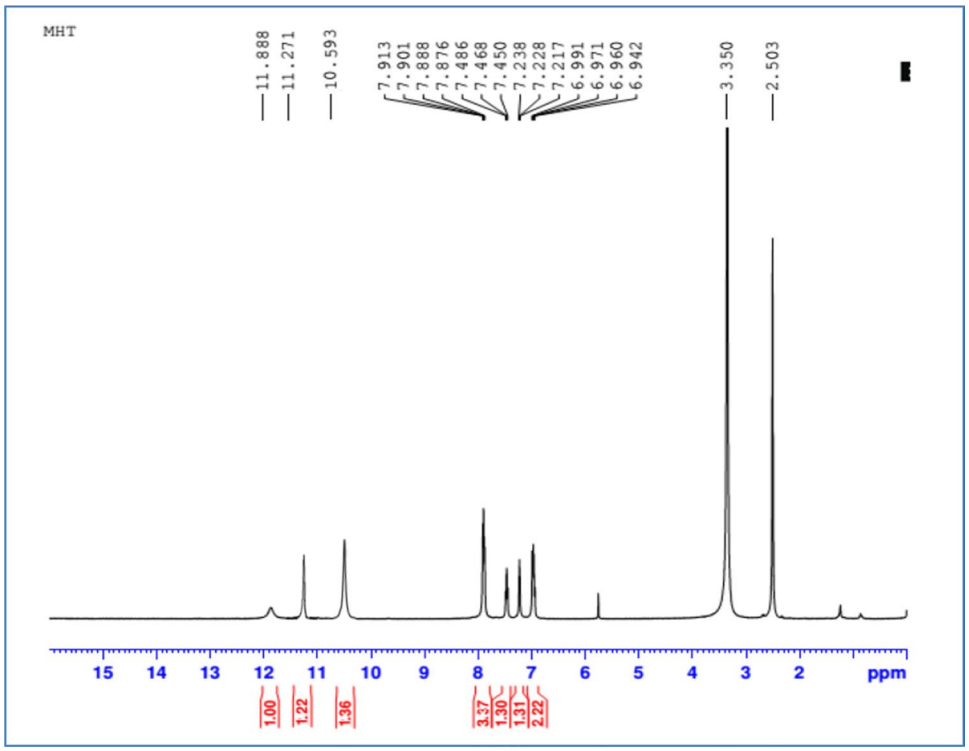

Fig. 3 ^{1}H NMR spectrum of ligand (HTC)

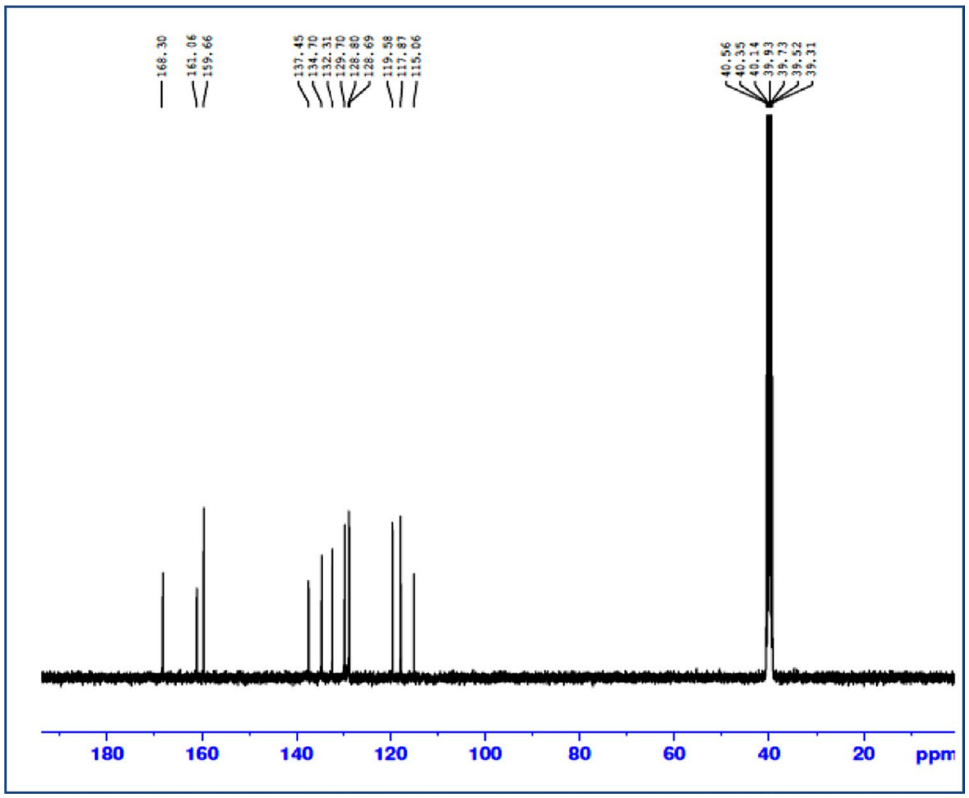

Fig. 4 ^{13}C NMR spectrum of ligand (HTC)

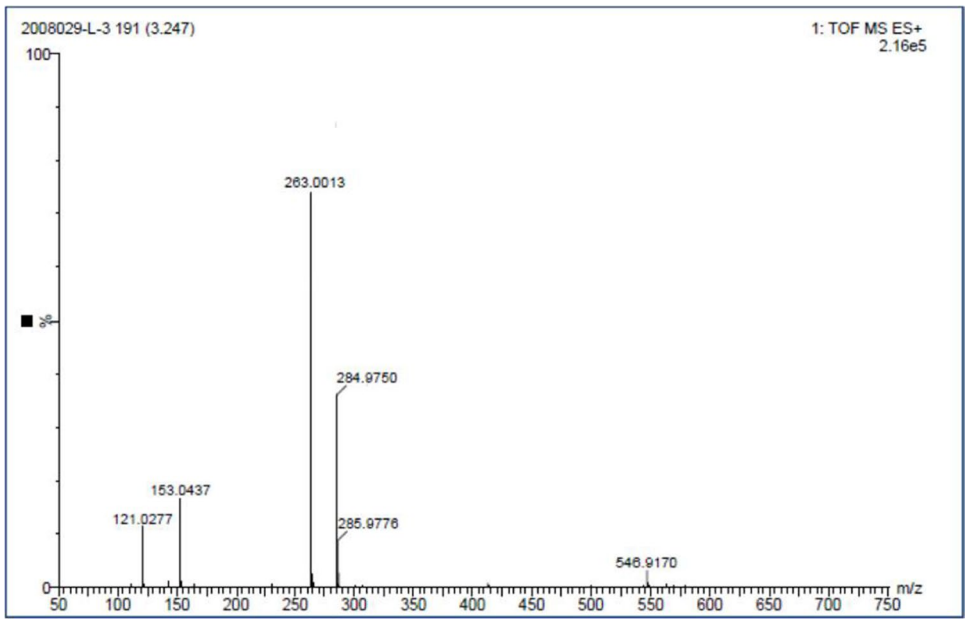

Fig. 5 LC–MS spectrum of ligand (HTC)

Cl_2], [Ni(HTC)$_2$.Cl_2], [Cu(HTC)$_2$.Cl_2], and [Zn(HTC)$_2$.Cl_2] exhibited molecular ion peaks [M + 1] *m/z* at 649.02, 649.18, 653.86, and 655.02 which were in accordance with the molecular weight of these complexes and also confirmed that the metal and ligand form the complexes in 1:2 ratio. The mass spectra of [Cu(HTC)$_2$.Cl_2] and [Zn(HTC)$_2$.Cl_2] are shown in Supplementary Figs. 1 and 2.

Table 2 FTIR spectral data (cm^{-1}) of HTC and its metal complexes

Compounds	ν(–OH)	ν(–NH)	ν(Ar–CH)	ν(C = O)	ν (C–S)	M–O	M–N
HTC	3429	3207	3014	1633	744	––	––
$[Co(HTC)_2.Cl_2]$	––	––	2368	1641	748	538	432
$[Ni(HTC)_2.Cl_2]$	––	––	2359	1637	748	540	430
$[Cu(HTC)_2.Cl_2]$	––	––	2336	1633	750	540	428
$[Zn(HTC)_2.Cl_2]$	––	––	2327	1630	750	540	430

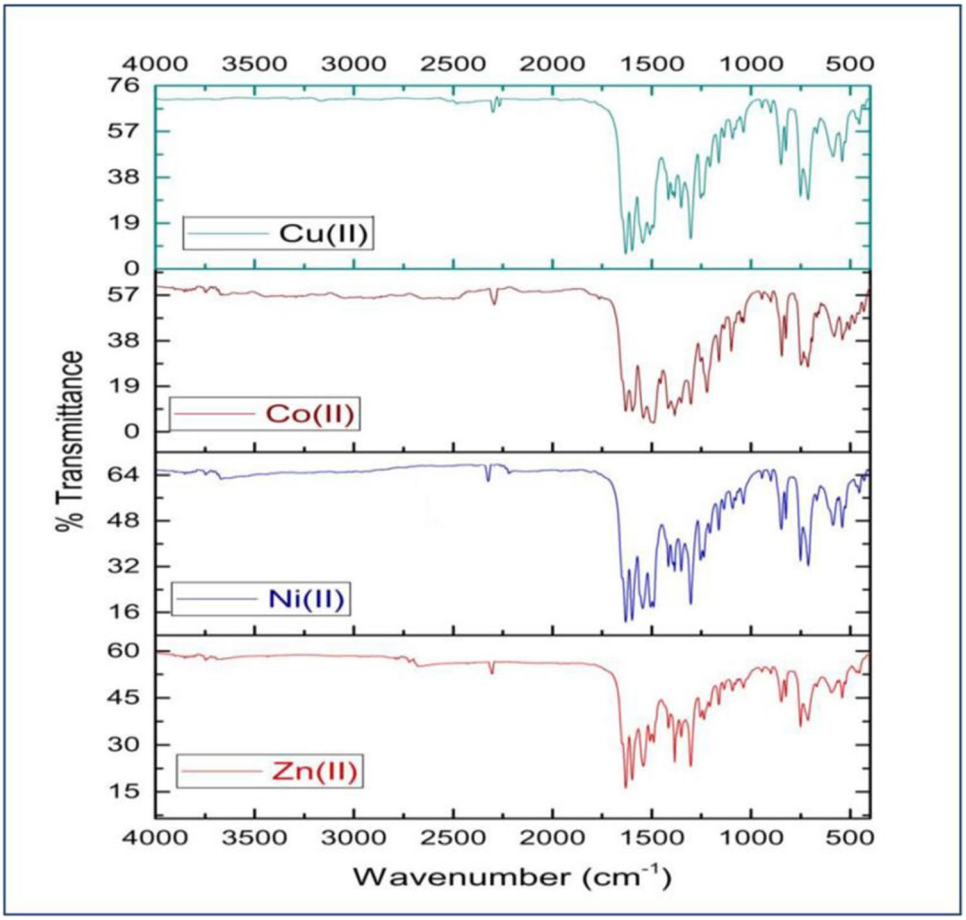

Fig. 6 FT-IR spectral of metal complexes

3.4 IR spectral studies

Prominent IR bands of the ligand and its metal coordinated compounds are enlisted in Table 2. The IR spectra of ligand are shown in Supplementary Fig. 3, whereas the IR spectra of transition metal complexes are shown in Fig. 6. In case of IR spectrum of the uncoordinated ligand, a broad peak was observed at 3429 cm^{-1} attributed to ν(–OH) stretching vibration, strong bands at 3207 cm^{-1} and 3016 cm^{-1} were correspondingly regarded to ν(–NH) and ν(Ar–CH) stretching vibrations. Further the free ligand also displayed two intense bands at 1633–1595 cm^{-1} because of the presence of ν(C = O) groups and a sharp band at 744 cm^{-1} due to ν(C-S) stretching vibration of the thiophene ring. But in case of IR spectrum of all the metal-coordinated compounds, the absence of (–OH) peak indicated the removal of proton of hydroxyl group attached to the benzene ring during the chelation, while the position of ν(C = O) bands remained unaltered justifying the non-indulgence of the ν(C = O) group in the coordination process. Also from the IR spectrum of synthesized metal-coordinated compounds, the absence of ν(–NH) bands was noticed and emergence of new peak at 1539–1547 cm^{-1} indicated the presence of –N = N– bond [26]. Further, the involvement of –N = N– group in the formation of complex was affirmed via appearance of new peaks at 432–430 cm^{-1} designated to ν(M–N) bonds and the bands obtained at 540–538 cm^{-1} was assigned to ν(M–O) bonds, respectively [27, 28].

Table 3 Electronic absorption spectral bands of metal complexes

Compound	Λ (nm)	Transitions	Magnetic moment (B.M)
HTC-1	619 708	$^4T_{1g}(F) \rightarrow 4A_{2g}(F)\ (\nu_1)$ $^4T_{1g}(F) \rightarrow {}^4T_{2g}(F)\ (\nu_2)$	3.77
HTC-2	479 514 618	$^3A_{2g}(F) \rightarrow {}^3T_{2g}(F)\ (\nu_1)$, $^3A_{2g}(F) \rightarrow {}^3T_{1g}(F)\ (\nu_2)$ $^3A_{2g}(F) \rightarrow {}^3T_{1g}(P)\ (\nu_3)$	2.86
HTC-3	538	$^2E_g \rightarrow {}^2T_{2g}$	1.78
HTC-4	-	-	Dia

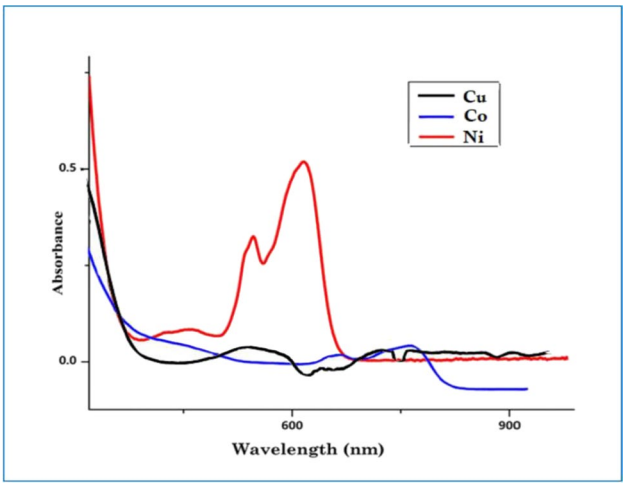

Fig. 7 Electronic absorption spectral bands of HTC metal complex

3.5 Electronic spectra and magnetic moment studies

The expected geometry of all the metal complexes were confirmed from their electronic absorption spectral study and magnetic susceptibility measurement data which are represented in Table 3 and Fig. 7. The electronic spectrum of the light green–colored Cu(II) complex displayed a wide peak at 538 nm attributing for $^2E_g \rightarrow {}^2T_{2g}$ transition and the magnetic moment value of 1.78 B.M. Hence an octahedral geometry was assigned to the aforesaid metal complex [29]. At 619 and 708 nm, the brown-colored Co(II) complex consisted of two absorption bands which are assignable to $^4T_{1g}$ (F) $\rightarrow 4A_{2g}$ (F) (υ_1) and $^4T_{1g}$ (F) $\rightarrow {}^4T_{2g}$ (F) (υ_2) transitions and the obtained magnetic moment value of 3.77 B.M suggests an octahedral coordination throughout the cobalt ion complex [30, 31]. In case of pale green–colored Ni(II) complex, three absorption shoulders were observed at 479, 514, and 618 nm allocated to $^3A_{2g}(F) \rightarrow {}^3T_{2g}(F)\ (\nu_1)$, $^3A_{2g}(F) \rightarrow {}^3T_{1g}(F)\ (\nu_2)$ and $^3A_{2g}(F) \rightarrow {}^3T_{1g}(P)\ (\nu_3)$ transitions with magnetic moment value 2.86 B.M indicating octahedral coordination, respectively [32].

3.6 Powder X-ray diffraction study

The powder XRD diffraction was determined for all the metal complexes of ligand HTC in the range $2\theta = 0$–$80°$, where the complexes displayed prominent sharp peaks specifying their crystallinity. The data obtained by the evaluation of diffraction patterns of the cobalt and copper complexes

Table 4 Powder XRD spectral data of Co(II) complex

Peak no	2θ	θ (degree)	θ (radian)	sinθ	*hkl*	*d*		*a* in Å
						Cal	Obs	
1	14.22703	7.113515	0.124	0.1237	111	6.220	6.187	5.65
2	15.10378	7.55189	0.131	0.1313	200	5.861	5.781	5.65
3	16.87434	8.43717	0.147	0.1466	210	5.249	5.231	5.65
4	22.4219	11.21095	0.195	0.1943	220	3.962	3.954	5.65
5	24.6825	12.34125	0.215	0.2136	300	3.604	3.598	5.65
6	26.1328	13.0664	0.227	0.2259	310	3.407	3.400	5.65
7	26.9097	13.45485	0.234	0.2325	311	3.310	3.301	5.65

Table 5 Powder XRD data of Cu(II) complex

Peak no	2θ	θ (degree)	θ (radian)	sinθ	*hkl*	*d*		*a* in Å
						Cal	Obs	
1	13.10303	6.551515	0.114	0.1140	111	6.751	6.740	3.62
2	14.15982	7.07991	0.123	0.1231	200	6.249	6.221	3.62
3	16.58181	8.290905	0.144	0.1441	210	5.341	5.328	3.62
4	21.49689	10.74845	0.187	0.1864	220	4.130	4.119	3.62
5	22.29812	11.14906	0.194	0.1932	300	3.983	3.964	3.62
6	25.12253	12.56127	0.219	0.2173	311	3.541	3.523	3.62
7	27.34862	13.67431	0.238	0.2362	320	3.258	3.228	3.62

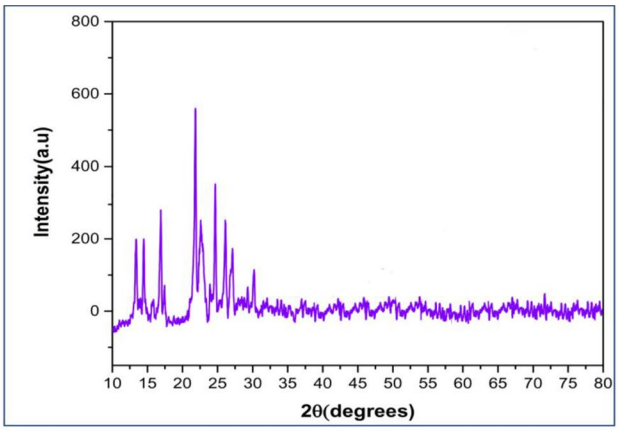

(a). Powder XRD pattern of Co(II) complex

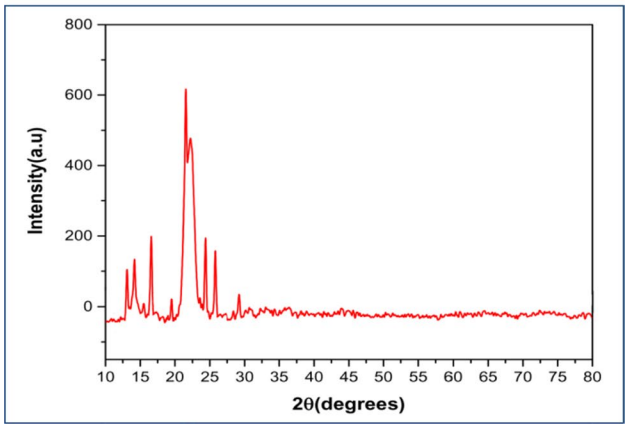

(b). Powder XRD pattern of Cu(II) complex

Fig. 8 **a** Powder XRD pattern of Co(II) complex**. b** Powder XRD pattern of Cu(II) complex

are summarized in Tables 4 and 5 and diffractograms are displayed in Fig. 8(a) and (b). The Miller indices (*hkl*) together with observed and determined interplanar space *d*, 2θ values were calculated and orthorhombic crystal system was confirmed for all the metal-coordinated compounds. The calculation of average crystallite sizes of the complex was carried out with Debye Scherrer equation ($D = K\lambda/\beta \cos\theta$), where *D* is the particle size, *K* is the dimensionless shape factor, λ is the X-ray wavelength (0.15406 Å), β is the line broadening at half the maximum intensity, and θ is the diffraction angle. The Co(II), Ni(II), Cu(II), and Zn(II) coordinated compounds have a crystalline size of 23.89 nm, 25.34 nm, 12.72 nm and 20.86 nm, which indicated the nanocrystalline phase of the coordinated compounds.

3.7 Thermal analysis

The thermal decomposition of Co(II), Ni(II) , Cu(II), and Zn(II)-coordinated compounds was analyzed with the aid of thermogravimetric method at the temperature range of 25–800 °C. The values of thermal stability have been indexed in Table 6 and shown in Fig. 9. Thermoanalytical curves including both Co(II) and Cu(II) complexes were obtained in two steps where Cu(II) complex showed first stage of degradation with a mass loss of 61.05% (cal: 62.87) indicating removal of organic moiety with two chloride ions ($C_{16}H_{12}N_4O_5Cl_2$) in the temperature range of 272–309 °C. The second stage of deterioration occurred in the range of 480–532 °C with a mass loss of 24.01% (cal: 24.92%) which can be related to the loss of two thiophene molecules leaving behind the stable CuO residue 12.05% (cal: 12.19%) in the temperature range of 638–744 °C.

Likewise, the thermoanalytical curve of Co(II) complex exhibited the first break down of complex molecule bearing a

Table 6 Decomposition steps and weight loss of metal complexes

Compounds	Decomposition steps	Temperature range (°C)	Removed species	Wt. loss (%) found (calculated)
$[Cu(HTC)_2.Cl_2]$	I	272–309	$-(C_{16}H_{12}N_4O_5Cl_2)$	61.05 (62.87)
	II	480–532	$-(C_8H_8S_2)$	24.01 (24.92)
	Residue	638–744	CuO	12.05 (12.19)
$[Co(HTC)_2.Cl_2]$	I	271–311	$-(C_{16}H_{12}N_4O_5Cl_2)$	62.10 (62.45)
	II	468–538	$-(C_8H_8S_2)$	25.04 (25.92)
	Residue	670–770	CoO	11.24 (11.56)
$[Ni(HTC)_2.Cl_2]$	I	269–305	$-(C_4H_4N_4O_4Cl_2)$	37.29 (37.34)
	II	342–355	$-(C_8H_8S_2)$	24.55 (24.76)
	III	470–562	$-(C_{12}H_{12}O)$	26.45 (26.57)
	Residue	681–755	NiO	11.07 (11.52)
$[Zn(HTC)_2.Cl_2]$	I	274–312	$-(C_4H_4N_4O_4Cl_2)$	36.85 (37.16)
	II	462–502	$-(C_8H_8S_2)$	23.99 (25.68)
	III	529–548	$-(C_{12}H_{12}O)$	26.32 (26.09)
	Residue	726–765	ZnO	12.05 (12.44)

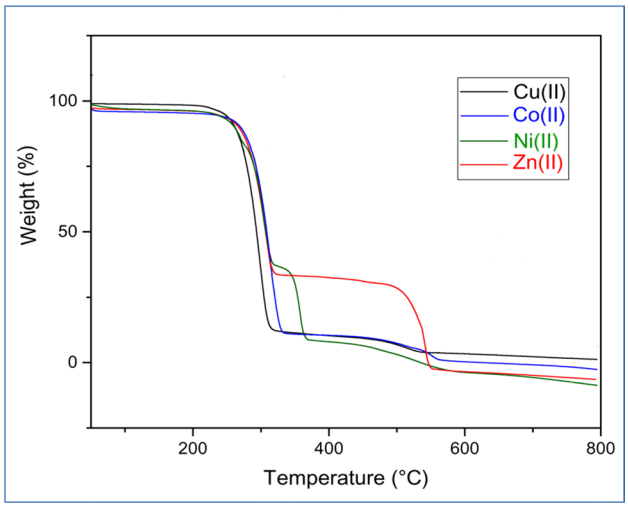

Fig. 9 Thermoanalytical curves (TGA) of the metal complexes

mass loss of 62.10% (cal: 62.45%) specifying the removal of organic moiety with two chloride ions ($C_{16}H_{12}N_4O_5Cl_2$) took place at 271–311 °C. The second TG curve was obtained in 468–538 °C range bearing weight loss of 25.04% (cal: 25.92%) suggesting the removal of two thiophene molecules leaving behind the stable CoO residue 11.24% (cal: 11.56%) correspondingly at the temperature range of 670–770 °C.

Whereas Ni(II)- and Zn(II)-coordinated compounds displayed the depletion pattern in three steps. Thermoanalytical curve of Ni(II) complex revealed the initial step of decomposition with a mass loss of 37.29% (cal: 37.34%) indicating the removal of organic moiety with two chloride ions ($C_4H_4N_4O_4Cl_2$) in the temperature range of 269–305 °C. The second break down of the metal complex occurred with a mass depletion of 24.55% (cal: 24.76%), suggesting the elimination of two thiophene nucleus in the temperature range of 342–355 °C. The third degradation resulted with a mass loss of 26.45% (cal: 26.57%) relating to the removal of benzene molecule in the temperature range of 470–562 °C, leaving behind stable NiO residue 11.07% (cal: 12.19%) in the temperature range of 681–755 °C. Similarly, Zn(II) complex was found to exhibit its initial TG curve with mass depletion of 36.85% (cal: 37.16%), suggesting the removal of organic moiety with two chloride ions ($C_4H_4N_4O_4Cl_2$) at the temperature range of 274–312 °C. The second step of decomposition occurred with a mass loss of 23.99% (cal: 25.68%), specifying the removal of two thiophene molecules in the temperature range of 462–502 °C. The third TG curve resulted with a mass elimination of 26.09% (cal: 26.32%) which can be considered the disappearance of benzene molecule in the temperature range of 529–548 °C, leaving behind stable ZnO residue 12.05% (cal: 12.44%) at the temperature range of 726–765°.

3.8 Kinetic studies

Several equations have been used for the kinetic studies of the thermal systems. Most of these equations represent relationship between mass and temperature which evaluates the degradation process. In the present work with the aid of Broido's method, kinetic parameters were examined from TGA curves. The plottings of ln(ln 1/*y*) versus 1000/*T* (where *y* is the fraction not yet decomposed) for various steps of thermal deterioration of coordinated compounds are illustrated in Supplementary Fig. Supplementary Figs. 4(i)–(iv) and the data are presented in Table 7.

The slope of the plot ln(ln 1/*y*) versus 1000/*T* is associated to the energy of activation as

$$E_a = -2.303 \times R \times \text{slope}$$

where *R* = gas constant.

The parameters enthalpy (ΔH^*), entropy (ΔS^*), and Gibbs free energy (ΔG^*) of activation were estimated via below detailed standard equations,

$$\Delta H * = Ea - RT_d$$

$$\Delta S * = \Delta H * /T - 4.576 \log T/K' - 47.22$$

Table 7 Thermodynamic data of the thermal decomposition of metal complexes

Compounds	Mid temp (K)	E_a (kJ/mol)	ln*A* min^{-1}	ΔH* (kJ/mol)	Δ*S** (kJ/mol)	Δ*G** (kJ/mol)
$[Cu(HTC)_2.Cl_2]$	522.45	13.946	8.611	11.872	− 154.928	50.519
	740.26	32.492	11.618	28.607	− 144.072	95.927
$[Co(HTC)_2.Cl_2]$	520.76	8.730	6.122	6.670	− 155.045	45.084
	743.43	20.283	8.129	16.372	− 146.988	85.475
$[Ni(HTC)_2.Cl_2]$	520.27	5.344	4.477	3.288	− 155.144	41.651
	609.24	25.533	11.507	22.737	− 151.260	73.597
	747.75	8.074	4.965	4.127	− 147.244	74.031
$[Zn(HTC)_2.Cl_2]$	524.24	13.371	8.302	11.282	− 154.842	50.184
	730.71	25.537	9.933	21.732	− 144.428	87.838
	802.11	593.274	138.682	588.875	− 131.687	658.552

where K'=-ln (ln 1/y)

$\Delta G* = \Delta H* - T\Delta S*$

From the obtained data, it was observed that the activation energies of decomposition were particularly in the ranges of 13.94–32.49, 8.73–20.28, 5.34–25.53, and 13.37–593.27 kJ mol^{-1} for Cu(II), Co(II), Ni(II) and Zn(II) complexes. The increase in the values of E_a indicates thermal stability of coordination compounds and positive values illustrated the occurrence of depletion reactions at a normal mode. The positive values of $\Delta G*$ in case of metal-coordination compounds suggest that the free energy of the final residue is greater than that of the first compound and every decomposition stage is non-spontaneous process. Further positive results of $\Delta H*$ meant that decomposition reactions are endothermic, and finally negative results of $\Delta S*$ suggested that the structures of activated complexes were more ordered than the reactants [33, 34].

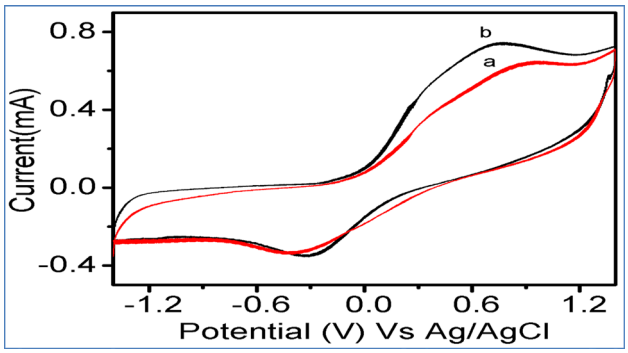

Fig. 10 Comparative cyclic voltammograms of **a** bare GCE and **b** Co(II)HTC/GCE) in 0.5 mM $K_4(Fe(CN)_6)$ scan rate = 50 mV/s

3.9 Electrochemical studies

3.9.1 Charge transfer behavior studies

The charge transfer behavior of Co(II)HTC electrode was examined via $K_4[Fe(CN)_6]$, which behaves as redox system. Bare glassy carbon electrode displayed ferri/ferrocyanide cyclic voltammetric response. The comparative cyclic voltammograms in 0.5 mM $K_4[Fe(CN)_6]$ solution at scan rate of 50 mV/s between bare GCE alongside modified Co(II) HTC/GCE electrodes are represented in Fig. 10. A pair of distinct reversible redox peaks were obtained by the CV of bare GCE in 0.5 mM $K_4[Fe(CN)_6]$ solution. An increase in both oxidation and reduction current was shown by the CV of Co(II)HTC/GCE-modified GCE compared to the bare GCE, which is possibly because of appreciable conducting properties of the cobalt complex and also it acts as good medium for electron transfer between buffer solution and GC electrode.

3.9.2 Electrochemical study of different electrodes

In phosphate buffer solution of pH-7, electrochemical sensing of DA and UA was studied due to the probable oxidation of these biomolecules in electrolytic solution. Since the reduction of molecular oxygen takes place at similar potential window, oxidation state was preferred. The CV of (a) Co(II) HTC/GCE (i) and Co(II)HTC/GCE for 0.5 µL concentration of DA (ii) and (b) Co(II)HTC/GCE (iii), Co(II)HTC/GCE for 01 µL concentration of UA (iv) at the scan rate 50 mV/s are represented in Fig. 11. The modified Co(II) complex electrode is commonly considered better physicochemical and electrochemical reactive metal complexes. Therefore, drop-coated modified Co(II)HTC/GCE exhibited intensified peak current responses as depicted in Fig. 11(i). Next for the concentration of DA at 0.5 µL, Co(II)HTC/GCE displayed current response which was studied and noticed that it exhibited quasi-reversible peak current response on its own peak

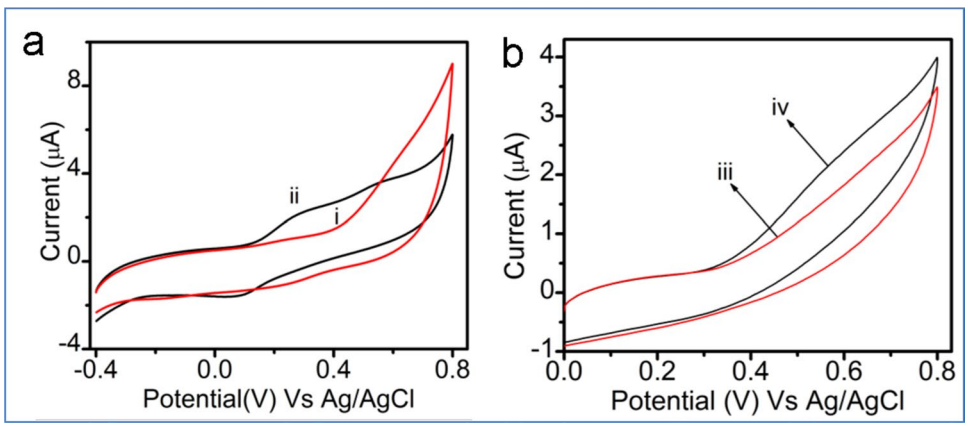

Fig. 11 Cyclic voltammogram of DA at **a** Co(II)HTC/GCE (i), Co(II)HTC/GCE for 0.5 µL concentration of DA (ii) and cyclic voltammogram of UA at **b** Co(II)HTC/GCE (iii), Co(II) HTC/GCE for 01 µL concentration of UA (iv), at the scan rate 50 mV/s

potential, as shown in Fig. 11(ii) and the modified GCE displayed peak current as shown in Fig. 11(b)(iii). Further on adding 1 µL UA at particular potential, the current peak was found to be enhanced, as presented in the Fig. 11(b)(iv).

3.9.3 Electrochemical study of dopamine

CV study of dopamine using modified Co(II) complex was carried out. The bare electrode did not show any peak current response while modifying the Co(II) complex to the GCE; the peak current obtained was 2.588×10^{-6} A. Thus, an intensified peak current was observed on its lower peak potential. Further toward the various concentration of DA (0.2–10 µM), the electrocatalytic response of Co(II)HTC/GCE was studied by cyclic voltammogram at a scan rate of 50 mV/s (Fig. 12). A precise and cosi-reversible peak current response occurred on its own peak potential of about + 295 mV upon adding varied concentration of DA from 0.2 to 10 µM, corresponding to the oxidation range of the dopamine. Upon investigation, it was noticed that by enhancing the amounts of DA, an increase in peak current response from 1.23×10^{-6} to 2.588×10^{-6} A was obtained. Between the peak current and concentration, a calibration graph was plotted as illustrated in Fig. 12. This suggested that modified Co(II) complex/GCE displayed better electrocatalysis activity with regard to the oxidation of dopamine. The calculated linear range, LOD and sensitivity is 0.2 to 10 µM/L, 0.06 µM, and 1.069 $\mu A \mu M^{-1}$ cm^{-2} and the correlation coefficient $R^2 = 0.9856$, respectively, justifies that the aforesaid modified electrode is a favorable material to sense dopamine.

3.9.4 Effect of scan rate (dopamine)

The effect of scan rate on Co(II)HTC/GCE was examined in buffer solution of pH-7, where it was noticed that by enhancing scan rate from 10 to 100 mV/s, peak current increased apparently as shown in Fig. 13. Between the peak current and square root of scan rate, a plot was formulated displaying linear relationship. This linear relationship indicated that oxidation of dopamine which occurred at modified Co(II) complex/GCE was a diffusion-controlled mass transfer reaction, as shown in Fig. 13(c), and with correlation coefficient of $R^2 = 0.993$.

3.9.5 Electrochemical determination of uric acid

The physicochemical activity of Co(II)HTC/GCE drop-coated electrode in the presence of various volume of UA was observed via cyclic voltammogram at a scan rate of 50 mV/s. Figure 14 depicts the various volumes of UA at modified electrode. Upon adding varied concentration of UA ranging from 0.1 to 0.8 µM, a proper defined redox peaks were obtained at 550 mV with the linear relationship between the *I*p and different volumes of UA. These observations recommended that the proposed electrode demonstrated appreciable physicochemical activity. The linear response of Co(II)HTC/GCE toward varying amounts of UA vs. cathodic peak current and the linear regression equation is (*I*pc); $Y = 5.1708$ (UA) + 1.30059 with correlation coefficient of $R^2 = 0.9974$ (inset Fig. 14b).

3.9.6 Effect of scan rate (uric acid)

CV was determined for 5 µL of UA in phosphate buffer solution of pH-7 at the scan rate 10–100 mV/s. The peak current was found to increase while enhancing the scan rate. A plot of *I*pa vs $\upsilon^{1/2}$ illustrated linear relationship specifying diffusion-controlled reaction, as represented in Fig. 15. The detection limit of 0.333 µmol/L, linear concentration range of 0.1–0.8 µmol/L and sensitivity of 5.170 $\mu A \mu M^{-1}$ cm^{-2} were obtained. Table 8 represents the comparative data of other modified electrodes along with the data obtained for

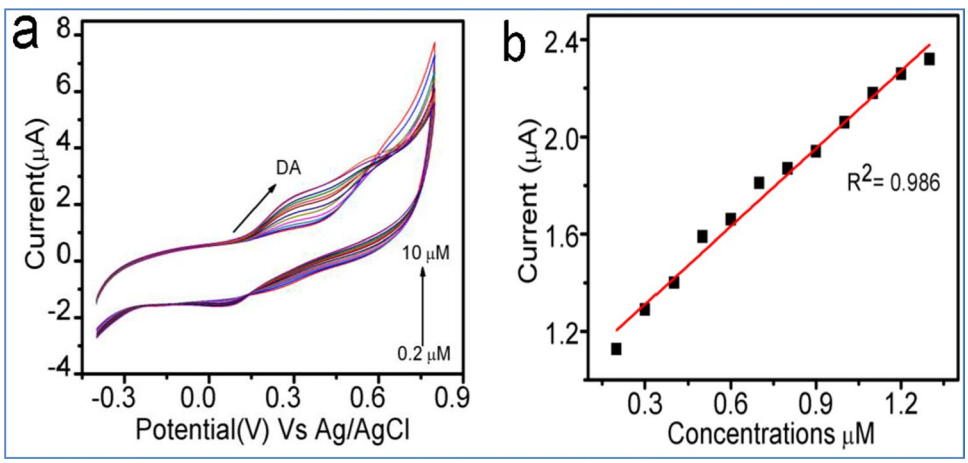

Fig. 12 **a** Cyclic voltammogram of DA at Co(II)HTC/GCE concentration ranging from 0.2 to 10 µM. **b** Inset calibration graph of current vs. DA concentration (µM)

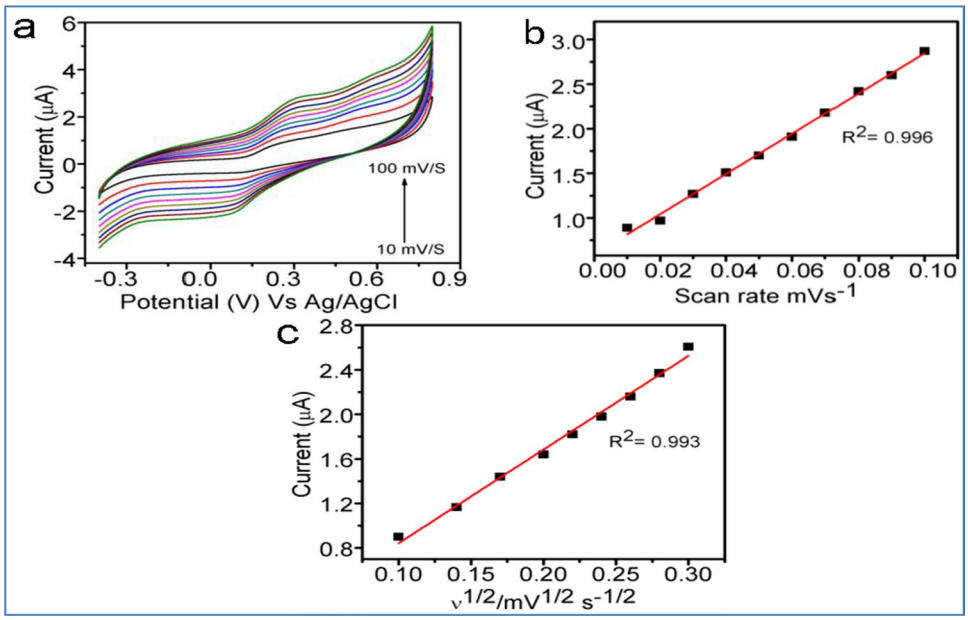

Fig. 13 The effect of scan rate on modified Co(II) HTC/GCE **a** cyclic voltammogram of dopamine at Co(II)HTC/GCE scanning rating ranging from 10 to 100 mV/s. **b** Inset calibration graph of current vs. scan rate and **c** the plot of current vs. $v^{1/2}$/ $mV^{1/2}$ $s^{-1/2}$

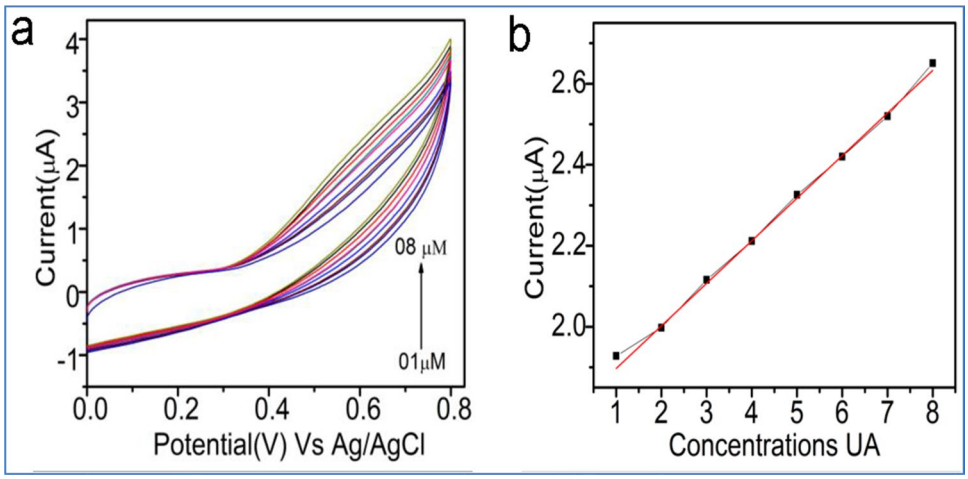

Fig. 14 Cyclic voltammogram plot of **a** Co(II)HTC/GCE at various concentrations (0.1–0.8 μM) of UA at scan rates 50 mV/s and **b** linear plot of peak current vs. different concentrations of UA

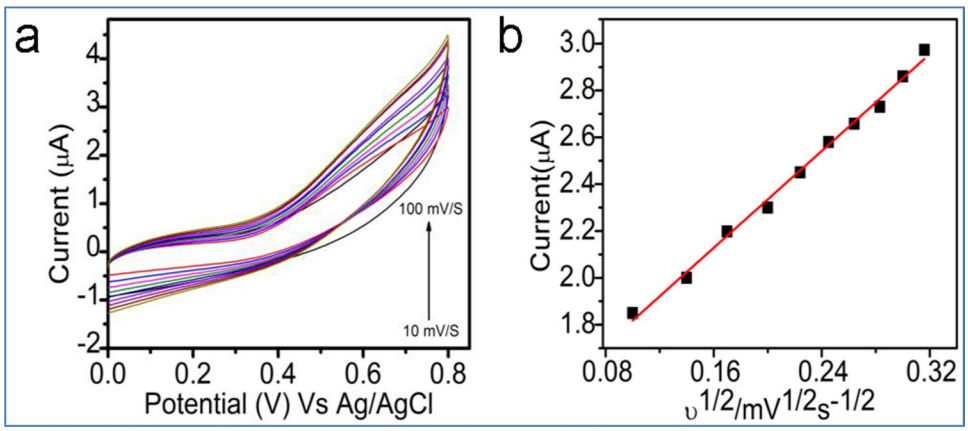

Fig. 15 Evaluation of cyclic voltammogram of **a** different scan rates of uric acid (10–00 mV/s) and **b** linear plot of peak current vs. square root of scan rates mV/s

Table 8 Comparison of modified electrodes

Electrodes	Detection methods	Samples	Linear range (μmol/L)	Sensitivity ($\mu A \mu M^{-1}$)	LOD (μmol/L)	Reference
GCE/rGO-Zn(II)TPEBiPc	CV	DA	0.2–10	2.173	0.066	35
rGo-Co_3O_4	CV	DA	0–30	0.389	0.0092	36
Azo-bridzed-CuPc polymer/GCE	CV	DA	10–160	0.078	0.33	37
GC_{OX}/nano-NiOx	SWV	DA	80–800	0.329	0.69	38
LaFeO3/ITO	CV	DA	5–200	-	0.006	39
Binuclear copper(II)-modified Au	DPV	DA	0.2–30	0.03	0.08	40
CoNSal/TOAB/CPE	CV	DA	01–100	-	0.5	41
Co(II) complex/GCE	CV	DA	0.3–3.9	0.532	0.1	42
Co(II)HTC/GCE	CV	DA	0.2–10	1.069	0.066	This work
Co(II)TPP-GCE	CV	UA	2–100	-	0.5	43
GO-ZIF67/GCE	CV	UA	0.8–200	-	0.001	44
Co(II)HTC/GCE	CV	UA	01–08	5.170	0.333	This work

Co(II)HTC/GCE, where it is evident that the modified Co(II) electrode used in the current research work displays noteworthy electrochemical performance for the detection of both the biomolecules like dopamine and uric acid [35–44].

3.9.7 Reproducibility and repeatability

The modified Co(II)HTC/GCE electrode was analyzed in four batches to ascertain reproducibility and also accuracy of determination. Uric acid and dopamine (0.5 μL) were detected by the modified Co(II)HTC/GCE electrode via cyclic voltammetry method. The RSD was estimated and found to be 2.1% for Co(II)HTC/GCE-modified electrode. The repeatability of sensor was carried out in order to detect the above-mentioned bioanalytes (0.5 μM) through reciprocating cyclic voltammetry analysis five times utilizing the same Co(II)HTC/GCE electrode. Further, the fabricated sensors displayed satisfactory reproducibility (2.3%) and repeatability (RSD – 1.6%).

3.9.8 Real-sample analysis

For the purpose of exploring the real-sample analysis of Co(II) HTC/GCE, we performed the analysis of DA and UA in human serum samples. From a hospital laboratory, the human blood samples were obtained; further they were subjected to centrifugation for 20 min to collect the upper serum. Dilution of procured serum was carried out through 10 repeated cycles with PBS pH-7, then perforated with standard concentration of DA (5, 10, 15 $\mu molL^{-1}$) and UA (10, 15, and 20 $\mu molL^{-1}$) considerably for affirmation. The standard addition process could be utilized for checking the exactness of analysis and the data retrieved is presented in Table 9. The recovery ranged from 97.46 to 106.08 and from 98.93 to 101.5 for DA and UA, respectively, which illustrated that aforesaid modified electrode can be successfully utilized for the investigation of biomolecules in human serum proving that the Co(II)HTC/GCE drop-coated sensor possessed significant practical applications.

Table 9 Real-sample analysis

Sample	Addition/ $\mu molL-^1$	Found/$\mu molL-^1$	Recovery %
DA	5.00	5.34	106.8
DA	10.00	9.94	99.4
DA	15.00	14.62	97.46
UA	10.00	10.15	101.5
UA	15.00	14.93	99.53
UA	20.00	19.67	98.93

3.10 Biological activity studies

3.10.1 Antimicrobial activity

The antimicrobial activities of synthesized ligand and its metal-coordinated compounds were performed, and it was observed that the metal-coordinated compounds were highly active when compared to the uncoordinated ligand. The values have been tabulated in Table 10 and depicted through Figs. 16(a) and (b). The HTC-1 and HTC-3 exhibited significant antimicrobial activity under alike experimental conditions for all the tested bacterial and fungal strains upon comparison to the remaining metal-coordinated compounds and uncoordinated ligand. Admirable biological activities showed by HTC-1 and HTC-3 are properly explained by chelation theory and the overtone concept [22]. Liposolubility being a predominant criteria for regulating both antibacterial as well as antifungal activity, upon coordination it substantially lessens

Table 10 Antimicrobial activity of HTC and its metal complexes inhibition zone in millimeters

Compound	Antibacterial activity								Antifungal activity			
	E. coli		*S. typhi*		*S. aureus*		*B. subtilis*		*A. niger*		*C. albicans*	
	100	200	100	200	100	200	100	200	100	200	100	200
HTC	11 ± 0.47	14 ± 1.15	12 ± 0.57	16 ± 0.47	10 ± 0.47	13 ± 0.57	11 ± 1.15	14 ± 1.52	09 ± 0.57	10 ± 1.15	10 ± 0.57	16 ± 0.47
HTC-1	15 ± 1.52	25 ± 1.15	12 ± 1.15	24 ± 1.52	13 ± 0.57	28 ± 1.15	14 ± 1.52	25 ± 0.57	13 ± 0.47	25 ± 1.52	14 ± 1.15	23 ± 1.52
HTC-2	13 ± 1.52	19 ± 1.15	13 ± 0.47	19 ± 0.57	11 ± 1.15	19 ± 0.47	12 ± 1.15	20 ± 1.15	11 ± 1.15	19 ± 1.52	13 ± 1.15	18 ± 1.15
HTC-3	14 ± 0.57	25 ± 0.47	15 ± 1.15	22 ± 1.52	18 ± 1.15	22 ± 1.52	15 ± 0.47	28 ± 1.52	14 ± 0.47	26 ± 0.57	12 ± 0.47	22 ± 1.52
HTC-4	11 ± 0.57	18 ± 0.47	11 ± 0.57	20 ± 0.47	12 ± 1.52	16 ± 0.57	12 ± 1.15	18 ± 0.47	11 ± 1.15	18 ± 0.47	11 ± 0.57	17 ± 1.15
Std 1	25 ± 0.47	28 ± 0.57	24 ± 0.57	27 ± 0.47	25 ± 0.57	30 ± 0.47	28 ± 1.15	34 ± 1.52	-	-	-	-
Std 2	-	-	-	-	-	-	-	-	26 ± 0.57	30 ± 0.47	22 ± 1.15	26 ± 1.52

*Std 1, chloramphenicol; Std 2, fluconazole

*Each value is expressed as mean ± SD of three replicates for the zone of inhibition

the polarity of the metal ion due to incomplete sharing of its positive charge with donor groups and it enhances *p*- and *d*-electron delocalization across the whole chelate ring. The chelation enhances the lipophilic property of metal ion being placed at the center which further favors its penetration across the lipid layer of the cell membrane. Further MIC study was accomplished for ligand and its metal complexes against bacterial strains as well as for fungal strains, where it was seen that HTC-1 and HTC-3 displayed potential values in comparison with that of free ligand and other metal-coordinated compounds. The comparative data of MIC are enlisted in Tables 11 and 12.

3.10.2 Antioxidant activity

DPPH radical scavenging activity is considered to be an ideal assay in evaluating the antioxidant activity, and this assay is the most widely utilized procedure for determining the oxidative potential of different metal complexes. 1,1-Diphenyl-2-picrylhydrazyl (DPPH) being a stable organic radical compound which reveals an intense purple color with an absorption maximum at 517 nm due to the existence of DPPH free radical. This radical, upon easily reacting with any compound that discharges a hydrogen atom or an electron, brings change in color from purple to yellow. The extent of discoloration suggests the scavenging ability of the compounds with respect to hydrogen donating ability. The antioxidant activity of ligand and synthesized metal-coordinated compounds have been examined for DPPH radical scavenging assay for varied concentrations (20–100 µg/mL) against BHT being utilized as a standard, and the values are indexed in Table 13 and represented in Fig. 17. The antioxidant activities for the synthesized ligand and its complexes were carried out as per the method discussed in the procedure section.

From the antioxidant activity data, it was observed that the metal complexes exhibited high radical scavenging activity than that of the ligand but less than BHT. The Cu(II) and Ni(II) complexes showed increased potent DPPH scavenging activity with good scavenging rates (31.11–85.32 and 33.28–89.71). The rest of the complexes displayed fairly good activity compared to unbounded ligand. Lastly, the intensified activity of the complexes could be regarded due to the electron withdrawal nature of Co(II), Ni(II), Cu(II,) and Zn(II) ions which regulates the discharge of hydrogen in order to reduce DPPH radical.

3.10.3 Molecular docking studies

For the thorough acknowledgement of the binding interactions of prepared HTC ligand and its complexes regarding the cytotoxic behavior, molecular docking study was carried out on the anticancer receptor having PDB id:2A91 with actinoin used as standard. The stability of the best docked pose of these complexes was investigated by identifying the hydrogen bonding interactions of the protein with complexes, which revealed the amino acids involved in hydrogen bond formation. Based on these factors, among all the complexes the Co(II) complex and Cu(II) complex have lowest binding scores of − 338.10 and − 342.15 kcal/mol when compared with the standard (− 235.99 kcal/mol) and the ligand (− 224.91 kcal/mol), as shown in Table 14. The Co(II) and Cu(II) chelates displayed various types of binding interactions (hydrogen bonding, Pi-Pi, Pi-alkyl, alkyl) with different amino acid residues present in the enzymes of the receptor and thus enables the above-mentioned complexes to form a good binding species for the anticancer receptor.

The Co(II) and Cu(II) complex interactions (Pi-Pi, Pi-alkyl, alkyl) with active sites of 2A91 receptor's amino acid residues are GLU40, LEU41, THR42, TYR43, LEU44, PRO45, THR46, ASN47, ALA48, PHE87, GLU88, ASP89,

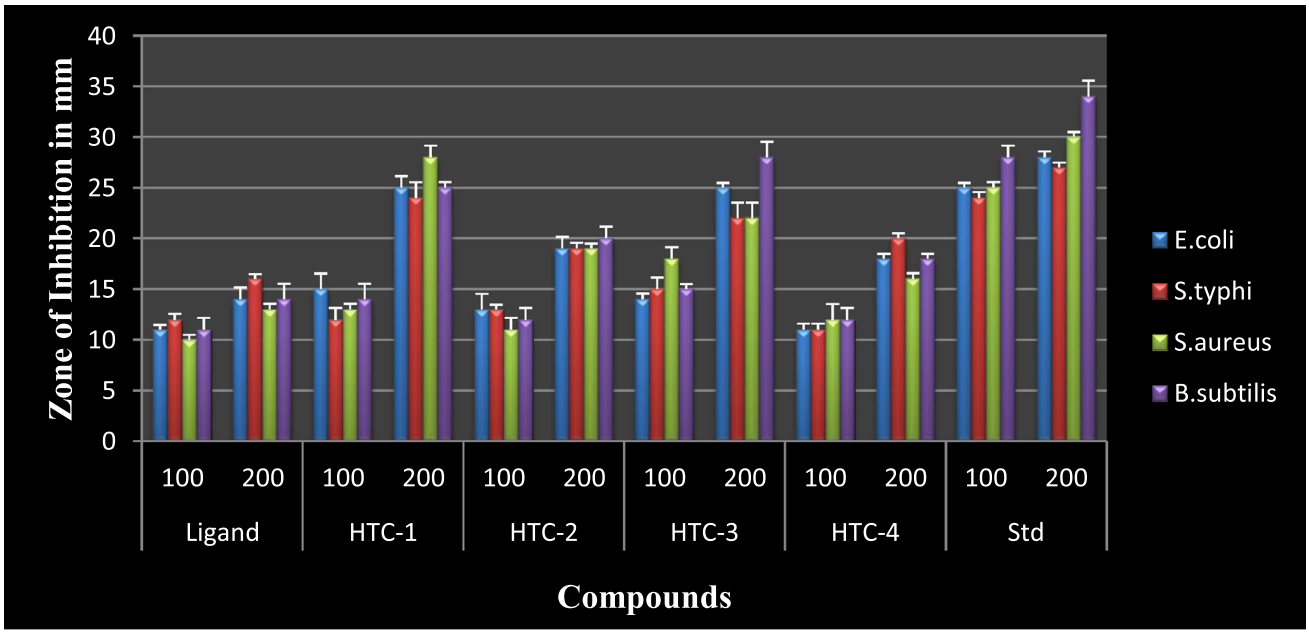

(a). Antibacterial activity of the HTC and its metal complexes

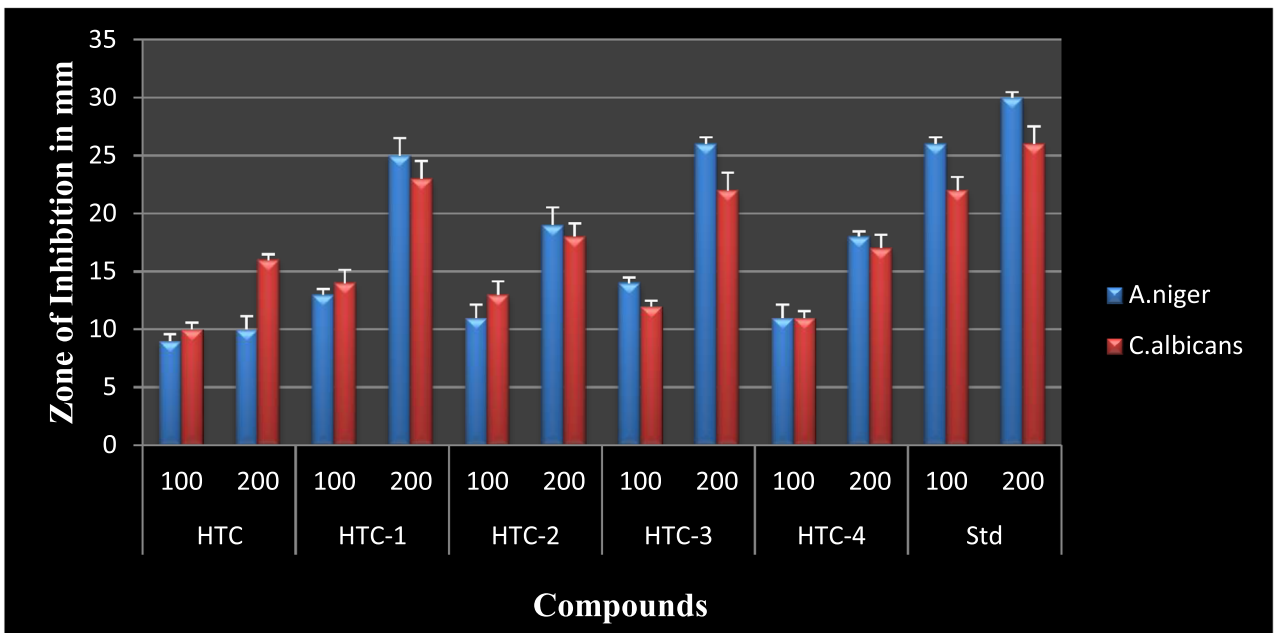

(b). Antifungal activity of the HTC and its metal complexes

Fig. 16 **a** Antibacterial activity of the HTC and its metal complexes. **b** Antifungal activity of the HTC and its metal complexes

ASN90, TYR91, ALA92, LEU93, TRP500, GLY501, PRO502, LEU86, PHE87, GLU88, and ASP89, ASN90, TYR91, ALA92, ASP510. The details of binding scores of ligand and the metals are enlisted in Table 14, and the 2D and 3D binding orientation of HTC (1–4) complexes with receptor 2A91 are illustrated in Fig. 18(a)–(d).

Table 11 MIC data of antibacterial activity of HTC and its metal complexes inhibition zone in mm

Compound	Antibacterial activity							
	E. coli				*S. aureus*			
	100	50	25	12.5	100	50	25	12.5
HTC	25 ± 0.47	23 ± 0.47	22 ± 0.47	23 ± 0.57	25 ± 0.47	23 ± 0.57	23 ± 1.15	22 ± 1.52
HTC-1	12 ± 1.15	12 ± 0.57	11 ± 0.47	12 ± 0.57	11 ± 0.47	12 ± 1.15	10 ± 0.47	11 ± 0.57
HTC-2	22 ± 0.47	21 ± 0.57	23 ± 1.15	23 ± 1.52	21 ± 0.47	20 ± 0.47	22 ± 0.57	23 ± 0.47
HTC-3	13 ± 0.47	12 ± 1.52	12 ± 0.47	13 ± 0.47	14 ± 0.57	13 ± 0.47	13 ± 0.57	12 ± 1.15
HTC-4	20 ± 1.15	19 ± 1.52	19 ± 1.15	18 ± 0.47	19 ± 0.57	20 ± 1.15	118 ± 0.47	18 ± 0.57
Std 1	08 ± 0.57	10 ± 0.47	10 ± 0.47	09 ± 0.57	10 ± 1.52	10 ± 0.47	09 ± 1.15	09 ± 0.47

*Std 1, chloramphenicol

*Each value is expressed as mean ± SD of three replicates for the zone of inhibition

Table 12 MIC data of antifungal activity of HTC and its metal complexes inhibition zone in mm

Compound	Antifungal activity							
	A. niger				*C. albicans*			
	100	50	25	12.5	100	50	25	12.5
HTC	26 ± 0.47	25 ± 0.57	25 ± 0.47	24 ± 0.57	25 ± 0.57	25 ± 1.15	24 ± 0.47	23 ± 0.57
HTC-1	13 ± 0.47	13 ± 0.47	11 ± 0.57	11 ± 1.15	14 ± 0.47	13 ± 0.57	13 ± 0.47	12 ± 0.57
HTC-2	22 ± 1.15	22 ± 0.47	21 ± 1.15	21 ± 0.47	23 ± 1.52	23 ± 0.47	22 ± 1.15	20 ± 0.47
HTC-3	14 ± 0.47	13 ± 0.57	13 ± 1.15	12 ± 0.57	12 ± 0.47	12 ± 0.57	11 ± 0.47	11 ± 0.57
HTC-4	21 ± 1.52	19 ± 1.15	19 ± 0.57	20 ± 1.15	18 ± 0.47	18 ± 1.15	19 ± 1.15	17 ± 0.47
Std 2	09 ± 0.57	09 ± 0.47	09 ± 0.57	08 ± 1.15	10 ± 0.57	10 ± 1.15	10 ± 1.15	08 ± 1.52

*Std 2, flucanazole

*Each value is expressed as mean ± SD of three replicates for the zone of inhibition

Table 13 Antioxidant activity of HTC and its metal complexes

Compounds	% of scavenging activity (concentrations in μg/mL)				
	20	40	60	80	100
HTC	22.91 ± 0.23	35.91 ± 0.23	45.39 ± 1.01	55.47 ± 0.28	61.37 ± 0.21
HTC-1	25.21 ± 0.21	46.32 ± 0.15	62.60 ± 0.27	67.02 ± 0.30	71.12 ± 0.14
HTC-2	33.28 ± 0.14	53.39 ± 0.20	71.19 ± 0.68	79.77 ± 0.42	89.71 ± 0.32
HTC-3	31.11 ± 0.31	51.11 ± 0.08	70.15 ± 0.20	77.19 ± 0.39	85.32 ± 0.20
HTC-4	27.15 ± 0.20	40.54 ± 0.30	55.33 ± 0.15	63.20 ± 0.27	70.55 ± 0.60
Std	39.14 ± 0.14	57.28 ± 0.17	79.34 ± 0.30	92.53 ± 0.27	97.56 ± 0.35

*Std, butylated hydroxytoluene

*Each value is expressed as mean ± SD of three replicates for the zone of inhibition

3.10.4 Cytotoxic studies

The encouraging results of molecular docking inspired the cytotoxic screening on four different cancer cell lines like human breast cancer (MCF-7), myelogenous leukemia (K-562), cervical cancer (HeLa), and kidney epithelial cells lacking interferons (Vero) under the similar condition tabulated in Table 15 and represented in Fig. 19. As a control, the untreated cells were utilized. Cell-growth inhibition was examined via MTT assay and the values revealed that the metal complexes showcased an inhibitory effect upon the multiplication of HeLa, MCF7, K-562, and Vero strain of cells in a dose-dependent method. The metal-coordinated compounds exhibited good score of inhibition over uncoordinated ligand HTC, signifying a probable synergistic effect upon ligand coordination to the metal ions. Upon screening, Co(II) and Cu(II) complexes displayed excellent inhibition scores of 90.35% and 88.31% for the lowest concentration (80, 90 μg/mL) for MCF-7 cell lines. Similarly aforesaid complexes exhibited the percent cell viabilities of 86.88%

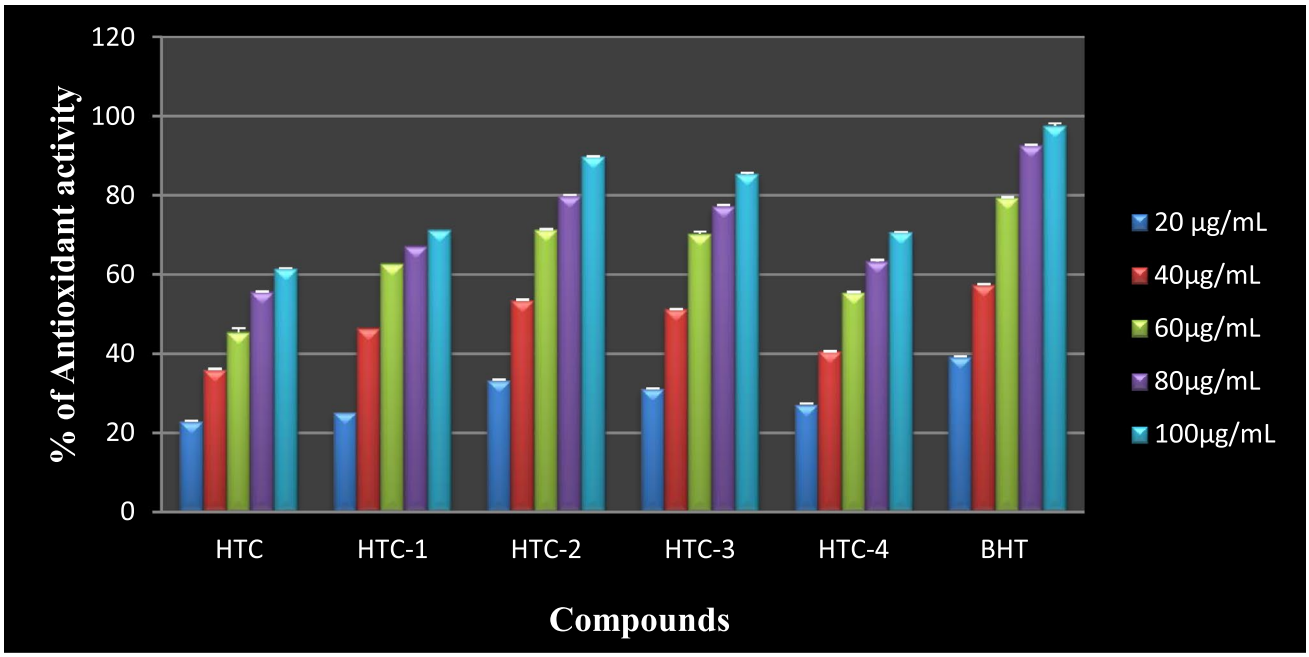

Fig. 17 Antioxidant activity of HTC and its metal complexes

Table 14 Molecular docking score of HTC and its metal complexes

Compounds	Receptor	E (kcal mol^{-1})
HTC	2A91	− 224.91
$[Co(HTC)_2.Cl_2]$	2A91	− 338.10
$[Ni(HTC)_2.Cl_2]$	2A91	− 317.68
$[Cu(HTC)_2.Cl_2]$	2A91	− 342.15
$[Zn(HTC)_2.Cl_2]$	2A91	− 308.10
Actinoin (STD)	2A91	− 235.99

and 89.23% for HeLa cell line for lowest concentration (80 µg/mL), respectively, while the moderate inhibition score was shown by these complexes for the other two cell lines (HeLa and Vero). Further, Ni(II) complex displayed an interesting cytotoxic rate of 72.58% at 90 µg/mL for K-562 strain of cells, and for Vero strain of cells it showed good inhibition rate of 83.64% at the concentration > 150 µg/mL. The inhibition statistics of Zn(II) complex outlines satisfactory inhibition score on the rapid multiplying of MCF-7, HeLa, K-562, and Vero strains of cells. Totally the cytotoxic activity of HTC and its complexes noticeably pointed out the essentiality of the coordination process on the biological properties.

4 Conclusion

The contemporary study highlights the biologically active Co(II), Ni(II), Cu(II), and Zn(II) complexes of novel *N*′-(3-hydroxybenzoyl)thiophene-2-carbohydrazide(L), which has been prepared and evaluated via different physicochemical as well as spectral approaches. Structural investigation of ligand and its metal-coordinated compounds was thoroughly done via various analytical techniques. The overall data is in favor with that of the proposed structure and suggested that the synthesized ligand forms a potential bidentate ligand and octahedral geometry is attributed to all the metal complexes. The electrocatalysis feature of the Co(II) complex was explored via electrochemical method by making use of Co(II)HTC/GCE toward varying amounts of DA and UA. The Co(II)-modified electrode showed impressive results including increased sensitivity, LOD, large concentration range, stability, and reproducibility properties.

The uncoordinated ligand and its metal-coordinated compounds were subjected for screening regarding antimicrobial, antioxidant, and cytotoxic activities. Further observed antimicrobial data indicated that the Co(II) and Cu(II) chelates were more biologically potent upon comparing with ligand and rest of the coordinated compounds. Whereas Cu(II) and Ni(II) chelates displayed considerable radical scavenging activity and further results of computational docking studies served as a motive force to examine the cytotoxic potency of ligand and its metal chelates for four different strains of cells where it was found that all the

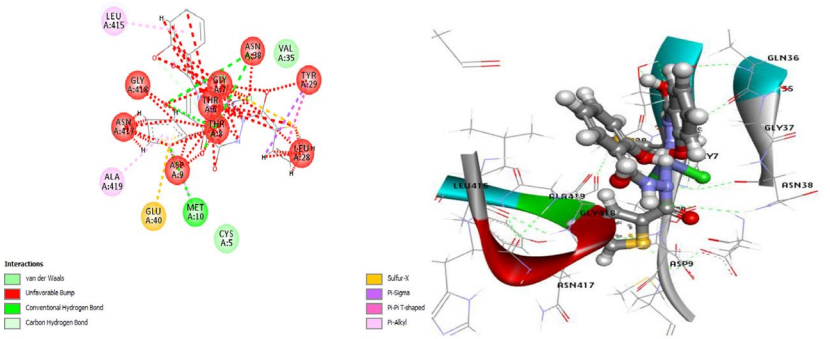

(a). 2-D and 3-D binding orientation of HTC-1 with receptor 2A91

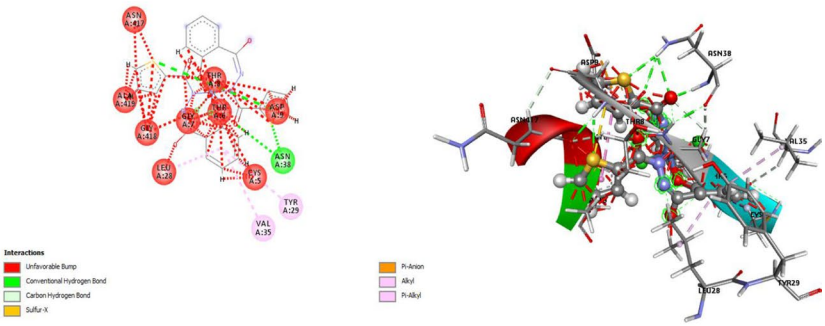

(b). 2-D and 3-D binding orientation of HTC-2 with receptor 2A91

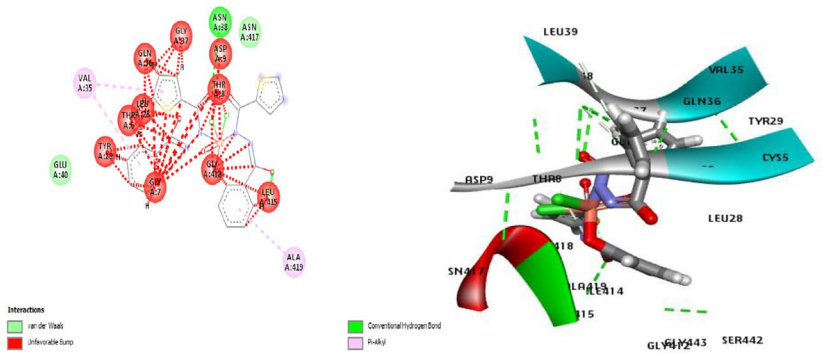

(c). 2-D and 3-D binding orientation of HTC-3 with receptor 2A91

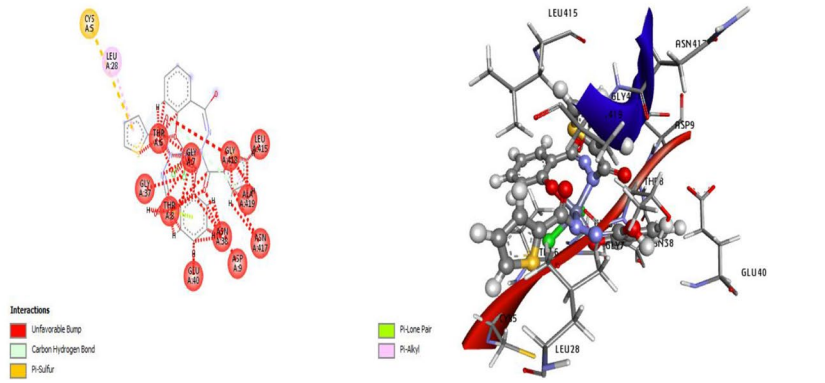

(d). 2-D and 3-D binding orientation of HTC-4 with receptor 2A91

Fig. 18 **a.** 2D and 3D binding orientations of HTC-1 with receptor 2A91. **b.** 2D and 3D binding orientation of HTC-2 with receptor 2A91. **c.** 2D and 3D binding orientations of HTC-3 with receptor 2A91. **d.** 2D and 3D binding orientations of HTC-4 with receptor 2A91

Table 15 Cytotoxic activity of HTC and its complexes

Compounds	MCF-7	HeLa	K-562	Vero
HTC	> 110 µg/mL 43.58 ± 0.11	> 110 µg/mL 49.25 ± 0.22	> 110 µg/mL 50.11 ± 1.25	> 150 µg/mL 52.38 ± 1.74
HTC-1	80 µg/mL 90.35 ± 0.22	80 µg/mL 86.88 ± 0.13	100 µg/mL 65.90 ± 0.36	100 µg/mL 75.82 ± 0.90
HTC-2	100 µg/mL 79.19 ± 0.33	110 µg/mL 78.88 ± 1.28	90 µg/mL 72.58 ± 0.65	> 150 µg/mL 83.64 ± 1.24
HTC-3	90 µg/mL 88.31 ± 0.18	80 µg/mL 89.23 ± 0.22	90 µg/mL 68.55 ± 0.11	100 µg/mL 78.79 ± 0.19
HTC-4	100 µg/mL 70.35 ± 1.35	90 µg/mL 84.18 ± 0.45	> 110 µg/mL 63.70 ± 0.19	> 150 µg/mL 82.44 ± 1.60

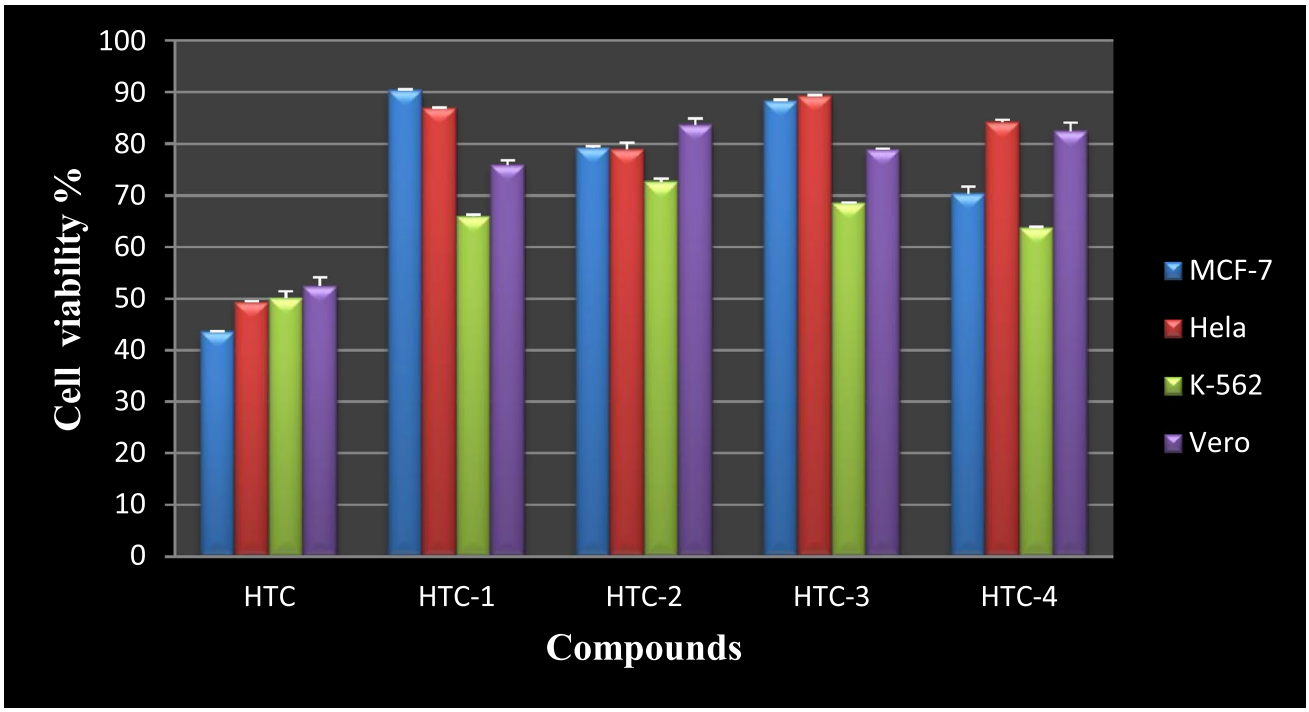

Fig. 19 Cytotoxic activity of HTC and its metal complexes

metal complexes exhibited remarkable cytotoxic potency when compared with the uncoordinated ligand.

Supplementary Information The online version contains supplementary material available at https://doi.org/10.1007/s42247-021-00312-4.

Acknowledgements The authors are grateful to the Directorate of minorities, Bangalore, Karnataka, India, for financial support. The authors are obliged to the Principal, JNNCE College and Principal, Sahyadri Science College, Shimoga for supporting the research work. We are also thankful to the Centralized Instrumentation Facility, Mysore University, SAIF, Karnataka University, Dharwad, Karnataka, India, for rendering both analytical and spectral data.

Declarations

Conflict of interest The authors declare no competing interests.

References

1. H. Benita Sherine, S. Veeramanikandan, Design, synthesis, structural elucidation and biological applications of benzohydrazide derivatives. Der Pharma Chem. **9**, 44–50 (2017)
2. P. Roy, B. Saikia, Cancer and cure: a critical analysis. Indian J. Cancer. **53**, 441–442 (2016). https://doi.org/10.4103/0019-509X.200658
3. M.J. Ahsan, J. Sharma, M. Singh, S.S. Jadav, S. Yasmin, Synthesis and anticancer activity of N-aryl-5-substituted-1,3,4-oxadiazol-2-amine analogues. J. Bio. Med. Res. Int. **9**, (2014). https://doi.org/10.1155/2014/814984
4. J.D.W. Van der Bilt, I.H.M. BorelRinkes, Surgery and angiogenesis. Biochim. Biophys. Acta (BBA) Rev. Cancer. **1**, 95–104 (2004)
5. S. Medici, M. Peana, V.M. Nurchi, J.I. Lachowicz, G. Crisponi, M.A. Zoroddu, Noble metals in medicine: latest advances. Coord. Chem. Rev. **284**, 329–350 (2014)

6. J. Martinez, A. Martinez, M.L. Cuenca, A.D. Lopez, Synthesis, thermal and spectral study of oxovanadium(IV) complexes with benzoic acid hydrazine and p-hydroxybenzoic acid hydrazid. Synth. React. Inorg. Met. Org. Chem. **18**, 881–901 (1988)
7. M.I. Saeed-ur-rehman, Sadia Rehman, Nazar-Ul-Islam, Nazir Jan, Synthesis and characterization of Ni(II), Cu(II) and Zn(II) tetrahedral transition metal complexes of modified hydrazine. J. Mex. Chem. Soc. **55**, 164–167 (2011)
8. N. Dodoff, K. Grancharov, N. Spassovska, Platinum(II) complexes of 4-methoxy-and 4-chlorobenzoic acid hydrazides. Synthesis, characterization and cytotoxic effect. J. Inorg. Biochem. **60**, 257–266 (1995)
9. R. Paprocka, Modzelewska-Banachiewicz, Bozena, Wiese, Małgorzata, Eljaszewicz, Andrzej, Michalkiewicz, Jacek, Synthesis and anti-inflammatory activity of hydrazide derivatives of 2-methylidene-1,4-dicarboxybutanoic acid. Acta Poloniaepharmaceutica. **69**, 1390–1394 (2012)
10. K.M. Khan, M. Rasheed, S. Zia-Ullah, F. Hayat, M.I. Choudhary. Kauka, S. Perveen. Atta-ur-Rahman, Synthesis and in vitro leishmanicidal activity of some hydrazides and their analogues. Bioorg. Med. Chem. **11**, 1381 (2003)
11. B.F. Abdel Wahab, H. Abdel Gawad, F.A. Badria. Ghada, Synthesis, antimicrobial, antioxidant, anti-inflammatory and analgesic activities of some new 3-(2,1-thienyl) pyrazole based heterocycles. Med. Chem. Res. **21**, 1418–1426 (2012)
12. C. Bonini, L. Chiummiento, M.D. Bonis, M. Funicello, P. Lupattelli, G. Suanno, F. Berti, P. Campaner, Synthesis, biological activity and modelling studies of two novel anti HIV PR inhibitors with a thiophenecontaining hydroxyethylamino core. Tetrahedron. **61**, 6580–6589 (2005)
13. G.J.M. Rejon, R.O.M. Castell, Synthesis and primary evaluation of the bactericide and fungicide activity of some 5-halofuranic and 5-halo-4-phenylthiazolic derivatives. Afinidad. **50**, 319–322 (1993)
14. V.U. Ahmad, N. Alam, New antifungal bithienylacetylenes from Blumeaobliqua. J. Nat. Prod. **58**, 426–1429 (1995)
15. T. Giridhar, R.B. Reddy, B. Prasanna, G.V.P. Chandra Mouli, Aminothiazoles: Part 1 Synthesis and pharmacological evaluation of 4-[isobutylphenyl]-2-substituted aminothiazoles. Indian J. Chem. **40**, 1279–1281 (2001)
16. N.K. Kaushik, H.S. Kim, Y.J. Chae, Y.N. Lee, G. Kwon, E.H. Choi, I.T. Kim, Synthesis and Anticancer Activity of Di(3-thienyl) methanol and Di(3-thienyl)methane. Molecules. **17**, 11456–11468 (2012)
17. Y.D. Wang, S. Johnson, D. Powell, J.P. McGinnis, M. Miranda, S.K. Rabindran, Inhibition of tumor cell proliferation by thieno[2,3-d]pyrimidin-4(1H)-one-based analogs. Bioorg. Med. Chem. Lett. **15**, 3763–3766 (2005)
18. L.D. Jennings, S.L. Kincaid, Y.D. Wang, G. Krishnamurthy, C.F. Beyer, J.P. McGinnis, M. Miranda, C.M. Discafani, S.K. Rabindran, Parallel synthesis and biological evaluation of 5,6,7,8-tetrahydrobenzothieno[2,3-d]pyrimidin-4(3H)-one cytotoxic agents selective for p21-deficient cells. Bioorg. Med. Chem. Lett. **15**, 4731–4735 (2005)
19. A.A. Ali AL-Riyahee, H.H. Hadadd, B.H. Jaaz, Novel Nickel(II), Copper(II) and Cobalt(II) complexes of Schiff bases A, D and E: Preparation, identification, analytical and electrochemical survey. Orient. J. Chem. **34**, 2927–2941 (2018)
20. N. Sunil Kumar, G. Krishnamurthy, M. Somegowda, M. Pari, T.R. RavikumarNaik, K.S. Jithedra Kumara, S. Naik, S. Kandagalla, N. Naik, Synthesis, characterization, electrochemistry, biological and molecular docking studies of the novel Co(II), Ni(II) and Cu(II) complexes derived from methane thiol bridged (2-((1H-benzo[d] imidazol-2-yl)methylthio)-1Hbenzo[d]imidazol-6-yl)(phenyl) methanone. J. Mol. Struct. **1220**, 128586 (2020)
21. Mounesh et al., Synthesis and characterization of tetra-ganciclovir cobalt(II) phthalocyaninefor eletroanalytical applications of AA/DA/UA. Heliyon. **7**, e01946 (2019). https://doi.org/10.1016/j.heliyon.2019.e01946
22. M.R. Lokesh, G. Krishnamurthy, H.S. Bhojyanaik, N.D. Shashikumar, P. Murali Krishna, DNA binding, In silico Docking and In vitro biological screening of some transition metal complexes of Schiff base ligand as potential blockers of cancer causing receptors. Int. J. Chem. Tech. Res. **6**, 150–162 (2014)
23. M.R. Lokesh, G. Krishnamurthy, R. Mohammed Shafeeulla, H.S. Bhojyanaik, P. Satapute, Evaluation of binding affinity with cancer causing receptors, CT-DNA and biological activities of mixed ligand complexes of some transition metal ions. J. Chem. Pharm. Res. **10**, 116–127 (2018)
24. R. Mohammed Shafeeulla, G. Krishnamurthy, H.S. Bhojynaik, T. Manjuraj, Synthesis, cytotoxicity, and molecular docking study of complexes containing thiazole moiety. JOTCSA. **4**, 787–810 (2017)
25. R. Mohammed Shafeeulla, G. Krishnamurthy, H.S. Bhojynaik, H.P. Shivarudrappa , Y. Shiralgi, Spectral thermal cytotoxic and molecular docking studies of N'-2-hydroxybenzoyl; pyridine-4-carbohydrazide its complexes. Beni-Suef Univ. J. Basic Appl. Sci. **4**, (2017). https://doi.org/10.1016/j.bjbas.2017.06.001
26. T.C.M. Yuvaraj, P. ParameshwaraNaik, G. Krishnamurthy, T.V. Venkatesh, R. Mohammed Shafeeulla, T. Manjuraj, Synthesis, characterization, XRD studies, molecular docking and biological screening of N-phenyl-2-(pyridin-4-ylcarbonyl) hydrazine carboxamide and their 3d metal ion complexes. Der Pharma Chem. **9**, 1–8 (2017)
27. S. Khan, S.A.A. Nami, K.S. Siddiqi, Synthesis, spectroscopic and thermal studies of transition metal complexes derived from benzil and diethylenetriamine. Spectrochim. Acta A. **68**, 269–274 (2007)
28. M.B. Halli, R.S. Malipatil, R.B. Sumathi, Preparation and characterization of Ni(II), Co(II), Cu(II), Cd(II), Zn(II) and Hg(II) complexes with schiff base derived from benzofuran-2- carbohydrazide and p-chloroacetophenone. J. Chem. Pharm. Res. **4**, 1259–1265 (2012)
29. H.O. Jamel, Shaimaa Adnan, Tariq Hussein Mgheer, Layth Sameer Jasim, Synthesis and characterization of the ligand (S, S'-Bis (benzo [d] Oxazol-2-yl) 2, 2'-((methylenebis (4, 1 phenylene)) bis (azanediyl)) diethanethioate (BMPAE) and it's complexes with some transition metals ions. J. Glob. Pharma Technol. **08**, 76–85 (2017)
30. M. Mokhles, A.A. Abd-Elzaher, H.A. Labib, S.A. Mousa, M.M. Moustafa, A.A. El-Rashedy. Ali, Synthesis, anticancer activity and molecular docking study of Schiff base complexes containing thiazole moiety. J. Basic Appl. Sci. **5**, 85–96 (2016)
31. A.S. Ramasubramanian, B. Ramachandra Bhat, R. Dileep, Synthesis, characterization and applications of metal complexes of 5-nitrosalicylidene 4-amino 3-mercapto-1, 2, 4-triazine- 5-one. Rasayan J. Chem. **3**, 122–126 (2010)
32. R.I.H. AL-Bayati, F.R. Mahdi, A.A.H. Al-Amiery, Synthesis, spectroscopic and antimicrobial studies of transition metal complexes of N-amino quinolone derivatives. Br. J. Pharm. Toxicol. **2**, 6–11 (2011)
33. H.A. Bayoumi, M.A. Alaghaz. Abdel-Nasser, MSh.. Aljahdali, Cu(II), Ni(II), Co(II) and Cr(III) complexes with N_2O_2-chelating Schiff's base ligand incorporating azo and sulfonamide moieties: spectroscopic, electrochemical behavior and thermal decomposition studies. Int. J. Electrochem. Sci. **8**, 9399–9413 (2013)
34. U.E. Ayaan, I.M. Gabr, Thermal, spectroscopic, and solvent influence studies on mixed-ligand copper(II) complexes containing the bulky ligand:Bis[*N*-(*p*-tolyl)imino]acenaphthene. Spectrochim. Acta A. **67**, 263–272 (2007)
35. M. Pari, K.R. Venugopala Reddy, K.B. Chandrakala. Fasiulla, Amperometric determination of dopamine based on an interface

platform comprising tetra-substituted Zn^{2+} phthalocyanine film layer with embedment of reduced graphene oxide. Sensors Actuators A. **316**, 112377 (2020). https://doi.org/10.1016/j.sna.2020.112377
36. A. Numan, M.M. Shahid, F.S. Omar, K. Ramesh, S. Ramesh, Facile fabrication of cobalt oxide nanograin-decoratedreducedgraphene oxide composite as ultrasensitive platformfor dopamine detection. Sensors Actuators B Chem. **238**, 1043–1051 (2017)
37. M. Pari, BS Jilani. Mounesh, K.R. Venugopala Reddy, Synthesis, spectral and electrochemical investigation of azo-bridged metallophthalocyanine polymer. Anal. Bioanal. Electrochem. **11**, 460–483 (2019)
38. Z.T. Althagafi, J.T. Althakafy, B.A. Al Jahdaly, M.I. Awad, Differential electroanalysis of dopamine in the presence of a large excess of ascorbic acid at a nickel oxide nanopartical-modified glassy carbon electrode. Hindawi J. Sensors. **2020**, 1–15 (2020)
39. Y. Kumar, S. Pramanika, Dipak Kumar Das, Lanthanum orthoferrite (LaFeO3) nano-particles based electrochemical sensors for the detection of dopamine. Biointerface Res. Appl. Chem. **10**, 6182–6188 (2020)
40. G. Jiang, Gu. Xuefang, G. Jiang, T. Chen, W. Zhan, S. Tian, Application of a mercapto-terminated binuclear Cu(II) complex modified Au electrode to improve the sensitivity and selectivity for dopamine detection. Sensors Actuators B. **209**, 122–130 (2015). https://doi.org/10.1016/j.snb.2014.11.109
41. S. Shahrokhian, H.R. Zare-Mehrjardi, Cobalt salpohen – modified carbon paste electrode incorporating a cationic surfactant for simultaneous voltammetric detection of ascorbic acid and dopamine. Sensors Actuators B. **121**, 530 (2007)
42. N. Sunil Kumar, G. Krishnamurthy, M. Somegowda, M. Pari, T.R. RavikumarNaika, K.S. Jithendra Kumara, S. Naika, S. Kandagalla, N. Naika, Synthesis, characterization, electrochemistry, biological and molecular docking studies of the novel Co(II), Ni(II) and Cu(II) complexes derived from methanethiol bridged (2-((1H-benzo[d]imidazol-2-yl)methylthio)-1H-benzo[d]imidazol-6-yl) (phenyl)methanone. J. Mol. Struct. **1220**, 128586 (2020)
43. L.I. Chun-Xiang, Z.E.N.G. Yun-Long, L.I.U. Ying-Ju, T.A.N.G. Chun-Rang, Simultaneous electrochemical determination of uric acid and ascorbic acid on a glassy carbon electrode modified with cobalt(II) tetrakisphenylporphyrin. Anal. Sci. **22**, 393–397 (2006)
44. J. Tang, Yu. Sixun Jiang, S.Z. Liu, L. Bai, J. Guo, J. Wang, Electrochemical determination of dopamine and uric acid using a glassy carbon electrode modified with a composite consisting of a Co(II)-based metalorganic framework (ZIF-67) and graphene oxide. Microchim. Acta. **185**, 486 (2018). https://doi.org/10.1007/s00604-018-3025-x